1 **Temperature-enhanced effects of iron on Southern Ocean phytoplankton**

3 Charlotte Eich[†,1,2,*], Mathijs van Manen[†,3], J. Scott P. McCain[4,5], Loay J. Jabre[4,6], Willem H. v.d. Poll[7], Jinyoung

4 Jung[8], Sven B. E. H. Pont[1], Hung-An Tian[3], Indah Ardiningsih[3], Gert-Jan Reichart[3,9], Erin M. Bertrand[4], Corina

5 P.D. Brussaard[1,2,*], Rob Middag[3, 10]

7 [†]These authors contributed equally to this work.

8 Affiliations:

9 [1] Department of Marine Microbiology and Biogeochemistry, NIOZ Royal Netherlands Institute for Sea Research,

10 1797 SZ 't Horntje, The Netherlands

11 [2]Institute for Biodiversity and Ecosystem Dynamics (IBED), University of Amsterdam, 1098 XH Amsterdam,

12 The Netherlands

13 [3]Department of Ocean Systems, NIOZ Royal Netherlands Institute for Sea Research, 1797 SZ 't Horntje, The

14 Netherlands

15 [4]Department of Biology, Dalhousie University, Halifax, Nova Scotia, Canada

16 [5]Current Address: Department of Biology and Department of Earth, Atmospheric, and Planetary Sciences,

17 Massachusetts Institute of Technology, Cambridge, MA 02142, USA

18 [6]Current Address: Marine Chemistry & Geochemistry Department, Woods Hole Oceanographic Institution,

19 Woods Hole, MA 02543, USA

20 [7]CIO Oceans, Energy and Sustainability Research Institute Groningen, Faculty of Science and Engineering,

21 University of Groningen, Nijenborgh 7, Groningen, AG 9747, The Netherlands.

22 [8]Korea Polar Research Institute, 26, Songdomirae-ro, Yeonsu-gu, Incheon 21990, Republic of Korea

23 [9] Department of Earth Sciences, Faculty of Geosciences, Utrecht University, Utrecht, the Netherlands

24 [10]Centre for Isotope Research-Oceans, Energy and Sustainability Research Institute Groningen, Faculty of Science

25 and Engineering, University of Groningen, 9712 CP Groningen, The Netherlands

27   *Correspondence to: Charlotte Eich (charlotte.eich@nioz.nl) & Corina Brussaard (corina.brussaard@nioz.nl)

Short summary

Phytoplankton growth in the Southern Ocean (SO) is often limited by low iron (Fe) concentrations. Sea surface warming impacts Fe availability and can affect phytoplankton growth. We used Fe clean shipboard incubations to test how changes in Fe and temperature affect SO phytoplankton. Their abundances usually increased with Fe addition and temperature increase, with Fe being the major factor. These findings imply potential shifts in ecosystem structure, impacting food webs and elemental cycling.

Abstract

Iron (Fe) is a key limiting nutrient for Southern Ocean phytoplankton. Input of Fe into the Southern Ocean is projected to change due to global warming, yet the combined effects of a concurrent increase in temperature with Fe addition on phytoplankton growth and community composition are understudied. To improve our understanding of how Antarctic phytoplankton communities respond to Fe and enhanced temperature, we performed four full factorial onboard bioassays under trace metal clean conditions with phytoplankton communities from different regions of the Weddell and the Amundsen Seas in the Southern Ocean. Treatments consisted of a combined 2 nM Fe addition with 2 °C warming treatment (TF), compared to the single factor treatments of Fe addition at *in-situ* temperature (F), and non-Fe addition at + 2 °C (T) and at *in-situ* temperature (C). Temperature had limited effect by itself but boosted the positive response of the phytoplankton to Fe addition. Photosynthetic efficiency, phytoplankton abundances, and chlorophyll *a* concentrations typically increased (significantly) with Fe addition (F and/or TF treatments) and the phytoplankton community generally shifted from haptophytes to diatoms upon Fe addition. The < 20 µm phytoplankton fraction displayed population-specific growth responses, resulting in a pronounced shift in community composition and size distribution (mainly towards larger-sized phytoplankton) for the F and TF treatment. Such distinct enhanced impact of Fe supply with warming on Antarctic phytoplankton size, growth and composition will likely affect trophic transfer efficiency and ecosystem structure, with potential significance for the biological carbon pump.

54   Keywords: Antarctic algae, bioassays, size-fractionation, climate change, trace metals

1. Introduction

The Southern Ocean plays an important role in regulating the Earth´s climate as it is an important sink for CO_2 (Takahashi et al., 2012; Friedlingstein et al., 2022; Fisher et al., 2023). Phytoplankton take up CO_2 and convert it to biomass, forming not only the base of the pelagic food web but also driving the biological carbon pump (Buesseler et al., 2020; Huang et al., 2023). During the short austral productive season, however, Antarctic phytoplankton growth often becomes limited by low iron (Fe) availability (Martin et al., 1990; Boyd, 2002; Ryan-Keogh et al., 2023). Fe is a vital micronutrient for a variety of cellular processes, including photosynthesis (Geider & La Roche, 1994; Schoffman et al., 2016; Kroh & Pilon, 2020) and nitrate assimilation (Schoffman et al., 2016). Shortage of Fe results in so called high nutrient, low chlorophyll (HNLC) conditions, where the ratio of macronutrients, especially nitrate, relative to total Chlorophyll a (Chl a) concentrations is comparably high (Minas & Minas, 1992; Sarmiento et al., 2004; Venables & Moore, 2010; Basterretxea et al., 2023). Trace metal supply in the Southern Ocean follows a strong seasonal cycle where in winter Fe is replenished via deep water-mixing (Tagliabue et al., 2014) or sediment resuspension in coastal areas (Boyd et al., 2012), but this supply is quickly depleted again by phytoplankton uptake in the next season. However, Fe limitation for Antarctic phytoplankton is predicted to be at least partially relieved in the future (Bazzani et al., 2023) because of enhanced Fe supply by increased wind driven mixing (due to reduced ice-induced stratification) and sources associated with ice melt, i.e., glaciers (Annett et al., 2015; Sherrell et al., 2015; Van der Merwe et al., 2019; L. Seyitmuhammedov et al., 2022) icebergs (Raiswell et al., 2008; Shaw et al., 2011; Raiswell et al., 2016; Hopwood et al., 2019) or sea-ice (Lannuzel et al., 2016; Gerringa et al., 2020). These changes in Fe supply are associated with ongoing climate change that is projected to lead to elevated temperatures and changes in wind patterns as well as associated currents and upwelling (Turner et al., 2005; Moore et al., 2018). Overall, future Southern Ocean conditions will most likely be warmer with potentially elevated Fe concentrations, which can be expected to also affect phytoplankton productivity and community composition (Boyd et al., 2015; Laufkötter et al., 2015, Pinkerton et al., 2021). Considering the urgency of warming and the anticipated change in Fe supply, there is a need for studies investigating the combined effects of these two important drivers controlling phytoplankton growth in the Southern Ocean. There are many reports on the effects of Fe addition to Fe-limited phytoplankton from the Southern Ocean (Reviewed by e.g. Yoon et al., 2018; Bazzani et al., 2023) and several on the influence of temperature (Reay et al., 2001; Morán et al., 2006; Boyd et al., 2013), but only few studies examined the combined effects of Fe and temperature on Antarctic phytoplankton (i.e. Rose et al., 2009; Zhu et al., 2016; Andrew et al., 2019; Jabre & Bertrand, 2020; Jabre et al., 2021; Aflenzer et al., 2023). In particular, studies using natural

85 phytoplankton communities are scarce (Rose et al., 2009; Jabre et al., 2021) and concentrated on Ross Sea

86 phytoplankton with relatively large temperature increases (3 to 6 °C). Hence, more insight into how phytoplankton

87 from other regional Antarctic seas respond to the warming projected by the year ~2100 (Meredith et al., 2019) is

88 needed.

89 The Weddell Sea is one of the key areas of dense Antarctic bottom water formation (Fahrbach et al., 2004) and

90 plays an important role in the global thermohaline circulation. The subpolar cyclonic Weddell Gyre circulating in

91 the Weddell Sea basin isolates the centre of the Weddell Sea from marginal Fe sources such as melt or sediments,

92 whilst the currents on the edges of the gyre have the potential to pick up Fe from a variety of sources, such as the

93 seafloor (Klunder et al., 2014; Sieber et al., 2021, Tian et al., in prep.). Generally, the Weddell Sea has a relatively

94 low primary productivity, associated with Fe limitation in the centre of gyre (Hoppema et al., 2007; Klunder et

95 al., 2014). In contrast, the west Amundsen Sea and specifically the Amundsen Sea Polynya (ASP) is known as

96 one of the most productive regions in the Southern Ocean in terms of net primary production per net area (Arrigo

97 & van Dijken, 2003). Additionally, this region (ASP) is characterised by a fast thinning of ice-sheets, shelf ice

98 and glaciers, with associated input of Fe required to sustain the high levels of primary productivity (e.g. Gerringa

99 et al., 2012; van Manen et al., 2022). Nevertheless, phytoplankton in the ASP could still be stimulated by

100 additional Fe input (Alderkamp et al., 2015).

101 The aim of the current study is to examine the concurrent effects of Fe supply and warming on Antarctic

102 phytoplankton communities from the Weddell Sea and the Amundsen Sea under controlled trace metal clean

103 conditions. Given the naturally low dissolved Fe (dFe) concentrations in the Southern Ocean, trace metal clean

104 conditions are crucial to avoid confounding Fe effects when studying temperature alone (Middag et al., 2023).

105 Our bioassay treatments comprised of Fe addition (F treatment), warming (T treatment), Fe addition and warming

106 (TF treatment) and the control (no Fe addition, no warming; C treatment). The temperature was enhanced by 2

107 °C, based on forecasts from the IPCC report (Meredith et al., 2019). Whilst the Amundsen Sea has shown a

108 warming trend over the past years already (Gómez-Valdivia et al., 2023; Drijfhout et al., 2024), the surface waters

109 of the Weddell Sea might not increase as much with climate change, but show short-term local temperature

110 increases (Darelius et al., 2023; Morrison et al., 2023; Teske et al., 2024). The concentration of dFe in the Fe

111 addition treatments (F and TF) was increased by 2 nM. Future Fe concentrations are highly uncertain (Hutchins

112 & Boyd, 2016; Tagliabue et al., 2016; Ryan-Keogh et al., 2023), and not necessarily linked to bioavailability of

113 Fe (Van Manen et al., 2022; Fourquez et al., 2023), but previous experiments in the Southern Ocean have shown

114 that such an addition represents (temporarily) Fe replete conditions (De Baar et al., 2005). Moreover, increased

115 Fe availability in the Southern Ocean could have a far-reaching impact, leading to increased nutrient consumption

116 consequently reducing nutrient transfer to lower latitudes where primary production is fuelled by these nutrients

117 (Primeau et al., 2013; Moore et al., 2018). By integrating biological and trace metal chemistry analyses within

118 large volume (20 L cubitainers), trace metal clean experiments, we aim to provide a clearer understanding of

119 future changes in phytoplankton growth patterns and the implications for the Southern Ocean's role in global

120 climate regulation.

121

122 **2. Material and Methods**

123 **2.1 Location and sampling**

124 Natural seawater for the bioassays was collected during research expeditions (Fig. 1) in the Amundsen Sea

125 (bioassays A1 and A2, R/V Araon, ANA08B, 2017/18) and in the Weddell Sea (bioassays W1 and W2, R/V

126 Polarstern, Alfred-Wegener-Institut Helmholtz-Zentrum für Polar- und Meeresforschung (2017), PS117,

127 2018/19) in austral summer (December – February).

128
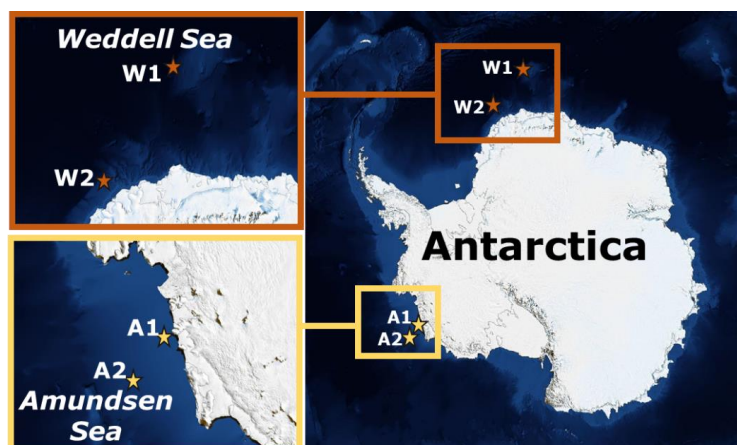
129

130 **Figure 1:** Location of the four bioassay experiments: Bioassays A1 and A2 were performed in the Amundsen Sea and W1 and
131 W2 in the Weddell Sea (Image obtained from NASA Worldview).

132

133 Seawater was sampled at the autofluorescence maximum (36 m for A2 and 20 m for both W1 and W2), except

134 for bioassay A1, which did not show an autofluorescence maximum and was sampled at the mid-mixed layer

135 depth (15 m). Water for each bioassay was collected in a single deployment of NIOZ's Titan ultraclean CTD

136 sampling system for trace metals (De Baar et al., 2008), mounted with pristine large volume samplers (Rijkenberg

137 et al., 2015). To prevent light shock for the phytoplankton, the original PVDF Pristine samplers were replaced by

138 a light-proof poly-propylene version. Salinity (conductivity), temperature, fluorescence, depth (pressure) and

139 oxygen were measured with a CTD (Seabird SBE 911+) mounted on the trace metal clean sampling system (De

140 Baar et al., 2008). To avoid contamination, further processing was performed under trace metal clean, dimmed

141 light conditions and at 2 °C in a cleanroom environment inside a modified high-cube shipping container which

142 fits the Titan sampling system.

143 Water for Amundsen Sea bioassay A1 was sampled from the middle of the Amundsen Sea Polynya (ASP) and for

144 bioassays A2 in the marginal sea ice zone just outside of the ASP. Both W1 and W2 were performed with water

145 from the eastern Weddell Sea. The Amundsen Sea bioassays A1 and A2 ran for 6 days (25 to 31 January and 31

146 January to 6 February 2018, respectively), whilst the Weddell Sea bioassays W1 and W2 ran for 8 days (28

147 December to 5 January and 9 to 17 January 2019, respectively). See Table 1 for *in-situ* environmental conditions

148 at sampling depth (at the start of the bioassays). The *in-situ* temperature was below zero for all bioassays, with

149 lowest values for A2 and W2 (-1.6 °C and -1.4 °C, respectively, compared to -0.6 °C and -0.3 °C for A1 and W1).

150 The daily average irradiance at sampling depth on day of sampling was lowest for A1 and A2, i.e., < 6 µmol

151 quanta m^{-2} s^{-1}, compared to 18 and 98 µmol quanta m^{-2} s^{-1} for W1 and W2.

152 **Table 1:** Characteristics of the seawater used for the bioassay experiments. Lat. = latitude, Long. = longitude, Temp =
153 temperature, Si = silicate, PO_4 = phosphate, NOx = nitrate + nitrite, Fe = iron, Chl a = chlorophyll *a*, Phyto = total flow
154 cytometry based phytoplankton abundances, F_v/F_m = photosynthetic capacity of the total phytoplankton. The reported
155 irradiance is the average irradiance at the sampling depth on the day of sampling.

Bioassay	Station	Lat.	Long.	Temp.	Salinity	Irradiance	Si
		(°S)	(°W)	(°C)	(psu)	(µmol quanta m^2 sec^{-1})	(µM)
A1	31	73.50	116.50	-0.6	33.99	5.0	84.7
A2	52	72.00	118.42	-1.6	33.89	3.1	78.5
W1	17	65.00	000.00	-0.3	33.90	17.7	58.3
W2	36	70.08	011.08	-1.4	33.82	97.6	27.7

Bioassay	PO_4	NOx	Fe	total Chl *a*	< 20 µm Chl *a*	Phyto	F_v/F_m
	(µM)	(µM)	(nM)	(µg L^{-1})	(%)	(x10^3 mL^{-1})	r.u.
A1	1.8	27.7	0.28	3.0	42	8.4	0.6
A2	2.1	30.9	0.10	0.4	98	7.1	0.6
W1	1.6	24.0	0.05	1.5	24	5.6	0.3
W2	1.9	27.9	0.03	0.6	65	4.4	0.3

156

2.2 Bioassay incubation set-up

157

158   Collapsible 20 L cubitainers (LDPE with PP caps and fitted with PE faucet; Cole-Palmer, Illinois, USA) were

159   used for the bioassay incubations. These were soap and HCL (1 M) cleaned prior to the expeditions and stored

160   with full surface contact in 0.024 M HCl (VWR Normatom Ultrapur, Avantor, Radnor, USA) for at least two

161   months. Before use, cubitainers were rinsed five times with ambient seawater. The natural seawater for the actual

162   incubations was distributed randomly to the total of 12 cubitainers which were then randomly assigned to the

163   different treatments. Trace metal clean conditions were maintained during all sampling and sample handling.

164   The bioassay treatments (performed in triplicate) were: *in-situ* conditions (control, C), + 2 nM dFe (as FeCl$_3$)

165   addition (F), + 2 °C temperature increase (T), and + 2 nM dFe addition and + 2 °C temperature increase (TF). For

166   the Amundsen Sea bioassays, a natural isotopic composition (natural dFe) was used for the dFe addition, whilst

167   d^{57}Fe was used in the Weddell Sea bioassays. This practice was adopted to better differentiate the added Fe from

168   the naturally present Fe, as we noticed that the dFe concentration in Fe amended Amundsen Sea bioassays quickly

169   returned to background concentrations (see section 3.1). Measuring Fe with a natural isotopic composition at these

170   low concentrations is still a challenge and combined with inherent variability between replicates. After several

171   days it became impossible to distinguish the Fe amended and non-amended treatments in Amundsen Sea bioassays

172   based on their natural dFe concentration (see section 3.1). The variation in natural dFe expected between Fe

173   amended and non-amended treatments despite precipitation and uptake, was hidden in the analytical and

174   environmental variability. For Weddell Sea bioassays we thus decided to add ^{57}Fe, a rare (2.12 % abundant *vs*

175   91.75 % for ^{56}Fe) natural isotope of Fe. Given its low natural abundance, ^{57}Fe is not nearly as sensitive to analytical

176   and replicate variation as such variation is insignificant relative to the addition, allowing better insight in Fe

177   drawdown over the course of the experiments.

178   Average starting concentrations of dFe in the Fe addition treatments ranged from 2.03 to 2.28 nM for both Weddell

179   and Amundsen Sea bioassays. Temperatures in the T and TF treatments were 1.4, 0.4, 1.7 °C and 1 °C, for A1,

180   A2, W1 and W2, respectively (see Table 1 for an overview of starting conditions in all treatments). One replicate

181   of the control treatment in bioassay W1 started leaking during the incubation and was thus not sampled from day

182   4 onwards. For bioassay W2, the *in-situ* temperature of -1.4 °C could not be maintained due to the very sunny

183   weather, resulting in an increase of 0.4°C for all treatments., Final incubation temperatures were -1.0 °C in the

184   control (C) and Fe-only (F) treatment and 1 °C (instead of 0.6 °C) in the T and TF treatments. This temperature

185   adjustment was done slowly over the course of 24 h on the second day of the incubation. More details about the

186 set-up can be found in the supplemental data (Fig. S1, supplement Bioassay Setup). Over the course of the

187 incubation period, temperatures were kept constant, with a maximum temperature fluctuation of ± 0.3 °C.

188 For Amundsen Sea bioassays, light levels were chosen to mimic *in-situ* conditions, but noting the low light

189 conditions during these incubations (ca. 3 % of in-air photoactive radiation, PAR; i.e. average 3.4 and 1.5 µmol

190 quanta m^{-2} s^{-1} for A1 and A2 over the course of incubation), we opted for non-limiting light conditions (Bertrand

191 et al., 2011) for the (later performed) bioassays of the Weddell Sea (ca. 12 % of in-air PAR; i.e. average 69 and

192 100 µmol quanta m^{-2} s^{-1} for W1 and W2 over the course of incubation). The percentages and values reported refer

193 to approximate light conditions within cubitainers. Samples for dissolved and particulate metals, Chl *a*, pigment-

194 based taxonomic analyses, and particulate organic carbon (POC), nitrogen (PON) and phosphate (POP) were

195 taken before filling of the cubitainers at the start of the bioassay incubations (t0), and at the end of the incubations

196 after 6 (Amundsen Sea) or 8 (Weddell Sea) days. Samples for phytoplankton photosynthetic efficiency (F_v/F_m)

197 and phytoplankton abundances were taken at least every other day. Macronutrients were measured on board at

198 least every other day to screen for potential macronutrient limitation.

199

200 **2.3 Setup verification**

201 To test for potential Fe contamination, three cubitainers were filled with ultrapure (UP) water and handled and

202 subsampled using the same methods and frequency as the treatments. Subsamples for dFe analysis were taken at

203 the start (0.08 ±0.04 nM) and after three (0.07 ± 0.04 nM) and six (0.06 ± 0.04 nM) days. Concentrations of dFe

204 stayed consistently low, suggesting minimal or no contamination. We also tested whether added dFe stayed in

205 solution or adsorbed to the cubitainer walls and found a slow gradual decrease over the first few days in dFe

206 concentrations after addition to UP water that we attribute to precipitation and wall adsorption (Table S1). During

207 our experiments, the concentrations of added dFe decreased more rapidly, whereas the dFe concentrations in the

208 non-Fe treatments, as well as the non-added form of dFe in Fe treatments ($d^{57}Fe$ for Amundsen and natural dFe

209 for Weddell Sea bioassays), stayed low and relatively constant over time. Since phytoplankton grew in all

210 treatments, the faster decrease of added dFe was likely due to uptake and sorption onto (biogenic) particles rather

211 than precipitation to the cubitainer walls. Low traceable amounts of $d^{57}Fe$ during the second half of the incubations

212 in W1 and W2 suggested that the initial decrease in Fe concentrations did not correspond to permanent removal

213 from the bioavailable Fe pool (e.g. due to absorption; Jensen et al., 2020) but instead buffered the dissolved pool

214 (as suggested for natural settings with exchange between the (labile) pFe and dFe pools; Van Manen et al., 2022),

215 or that most of the added Fe was taken up by phytoplankton as rapid luxury uptake during the first days of an

216 experiment (Lampe et al., 2018).

217

218 **2.4 Macronutrients**

219 During the Amundsen Sea bioassays, dissolved macronutrients were measured onboard following Jeon et al.

220 (2021), according to the Joint Global Ocean Flux Study (JGOFS) protocols (Gordon et al., 1993) using a four-

221 channel Auto-Analyzer (QuAAtro, Seal Analytical, Norderstedt, Germany). Measurement precisions were ± 0.02,

222 ± 0.28 and ± 0.14 µM for phosphate, silicic acid, and nitrogen (nitrate + nitrite), respectively (Jeon et al., 2021).

223 For Weddell Sea bioassays, samples for nitrate, nitrite, phosphate, and silicic acid were measured following the

224 method described by Gerringa et al. (2019). Measurements precisions were ± 0.01, ± 0.31 and ± 0.04 µM for

225 phosphate, silicic acid, and nitrogen (nitrate + nitrite), respectively.

226

227 **2.5 Dissolved and particulate metals**

228 Cubitainers were subsampled for dFe as well as other dissolved trace metals (dMn, dCo, dCu, dNi, dZn, dCd)

229 using a 0.2 µm Sartobron-300 filter cartridge (Sartorius AG, Göttingen, DE) for bioassay A1 and A2 and pre-acid

230 cleaned 0.2 µm Acropak filter cartridges (Cytiva, Marlborough, USA) for W1 and W2. Filters were fitted to an

231 UP-cleaned vented PE faucet attached to the cubitainer with HCl acid (1.5 M) cleaned silicon tubing. Filtered

232 samples were taken by applying pressure to the cubitainer. Different filters were used for Fe replete and deplete

233 treatments, and filters were replaced between experiments. The dissolved trace metal samples were collected in

234 acid cleaned 125 mL LDPE bottles following GEOTRACES protocols (Cutter et al., 2017) and directly acidified

235 by adding ultra-pure HCl (Baseline®HCl; Seastar Chemicals Inc, Sidney, CA), resulting in a concentration of

236 0.024 M with a final pH of ~1.8. Samples were stored until analysis at NIOZ. Trace metal samples were prepared

237 and analysed following van Manen et al. (2022) and references within. In short, trace metal samples were

238 preconcentrated using a SeaFAST pre-concentration system (ESI). Blank contributions from sample handling,

239 pre-concentration, and analysis steps were determined by analysing acidified MQ water (~1.8 pH) prepared in the

240 same way as real samples.

241 For particulate trace metals (pMn, pCo, pCu, pNi, pZn, pCd) and POP, 25 mm poly-ether-sulfone (PES) disc

242 filters (0.45 µm Pall Supor, Port Washington, USA) and polypropylene filter holders (Advantec, Cole-Parmer,

243 Vernon Hills, USA) were used, following the protocol adapted by Van Manen et al. (2022) with one additional

244 step: samples were soaked for at least 30 minutes in oxalate-EDTA (respectively 0.75M and 5.5M) in a 10L carboy

245   (VWR Collection; Avantor, Radnor, USA) to remove all trace metals outside or adsorbed to phytoplankton cell

246   walls (modified after Hassler & Schoemann, 2009) and subsequently filtered. Due to time limitations, samples for

247   particulate metals were only taken during experiment A1, W1 and W2. Filters were stored frozen at -20 °C until

248   analysis. In the NIOZ lab, filters were treated with two successive digestion steps to determine the total particulate

249   fraction. All vials used in the digestion procedures were rigorously cleaned with HF and HCl beforehand and

250   rinsed with UP water. Filters were subjected to a leach consisting of 1.8 mL of 4.35M (25 %) two times sub-boiled

251   distilled acetic acid and 0.02M (2 %) hydroxylamine hydrochloride (99.999 % trace metal basis, Sigma-Aldrich,

252   Saint-Louis, USA). Subsequently, filters were digested following the total digestion protocol developed by Cullen

253   & Sherrell (1999) and modified by Planquette & Sherrell (2012). A volume of 2 mL of 3 × sub-boiled distilled

254   8.0 M (50 %) HNO_3 (VWR Chemicals – AnalaR NORMAPUR, Avantor, Radnor, USA) and 2.9 M (10 %) HF

255   (Merck – Supelco, Kenilworth, USA) was added. The vials were closed tightly and refluxed for 4 h at 110 °C.

256   The solution was then transferred to a secondary Teflon vial and were then heated to near dryness at 110 °C. A 1

257   mL volume of 8.0 M (50 %) 3× sub-boiled distilled HNO_3 (VWR Chemicals– AnalaR NORMAPUR, Avantor,

258   Radnor, USA) and 15 % H_2O_2 (Merck – Suprapur, Kenilworth, USA) was added to the dried vial contents. The

259   vials were refluxed for 1 h at 110 °C and subsequently cooled to room temperature. Addition of reagents and

260   refluxing were repeated once. After this repetition, the vials were heated to near dryness at 110 °C. The samples

261   were re-dissolved in 2 mL 1.5 % 3× sub-boiled distilled HNO_3 with 10 ppb Rh as internal standard and transferred

262   to 2 mL Cryovials® (VWR, Avantor, Radnor, USA) for storage and analysis.

263

264   **2.6 ICP-MS trace metal measurements and particulate organic phosphorous**

265   Dissolved trace metal samples were preconcentrated using a SeaFAST pre-concentration system (ESI) using two

266   loops of 10 mL and were eluted into 350 µL elution acid (1.5 M Teflon distilled HNO_3 with rhodium as internal

267   standard) which gives a pre-concentration factor of 57.14 (see van Manen et al., 2022). Dissolved trace metal

268   samples, blanks (Supplementary Table S2), and references (Table S3) were analysed by ICP-MS (Thermo

269   Scientific Sector Field High-Resolution Element 2, Thermo Fisher-Scientific, Waltham, USA). Blank values were

270   much lower than the analysed samples, and reference results were in good agreement with certified values.

271   For the particulate samples, including POP, the procedure blanks without a filter were treated identically to the

272   samples, except for the steps involving filter handling and the removing of the filter from the filter holders.

273   Therefore, the vial blank is included in this reagent blank. Filter blanks consisted of unused acid cleaned PES disc

274   filters (Table S4).

275 Accuracy and precision of the digestions were assessed by Certified Reference Materials (CRMs). There is no

276 CRM available for marine suspended particulate matter, therefore accuracy could only be approximated by

277 analysis of other available CRMs. PACS-2 and MESS-3 (marine sediments, National Research Council of

278 Canada) were analysed. For each CRM, 10-30 mg were digested, whilst recommended sample weights are 250

279 mg for PACS-2 and MESS-3. The lower sample weights in this study were chosen to be representative of actual

280 marine particulate suspended matter concentrations (similar to Ohnemus et al., 2014). PACS-2 and MESS-3 were

281 only subjected to the total digestion (Table S5). The CRMs were in good agreement with the certified values.

282

283 2.7 Particulate organic carbon and nitrogen

284 For POC and PON sampling, 1 L of unfiltered seawater was collected from each cubitainer and stored in dark

285 bottles (Nalgene, Rochester, USA) at 1 °C until further processing (within 4 h after sampling). Filtrations were

286 then performed using combusted (4 h at 500 °C; Verardo et al., 1990) 0.3 µm 25 mm GF75 filters (Whatman,

287 Cytiva, Maidstone UK) and under modest under pressure (max. 200 mbar). Filters were folded once, packed in

288 aluminium foil, and stored frozen (-20 ºC) until analysis. The POC and PON concentrations were measured using

289 a Thermo-Interscience Flash EA1112 Series Elemental Analyzer (Thermo Scientific, Waltham, USA) with excess

290 oxygen, at 900 °C and a detection limit of 100 ppm and a precision of 0.3 % (Verardo et al., 1990). Before analysis,

291 GF75 filters were folded and packed into a tin cup. The instrument blank is included by the analyser calibration.

292 Carbon and nitrogen content of samples and blanks were computed according to the results of the standard

293 measurements, and the blank was subtracted from the sample. Acetanilide (C_8H_9NO) with 71.09 % C and 10.36

294 % N (ThermoQuest, Milan, Italy) was measured as standard material, and silty and sandy soil standards from

295 Elemental Microanalysis were measured as an internal reference.

296

297 2.8 Phytoplankton photosynthetic efficiency

298 F_v/F_m was determined in a Water-K quartz cuvette (3.5 mL) using pulse amplitude modulated fluorometry (Heinz

299 Walz WATER-PAM, with Red LEDWATER-ED cuvette version S/N EDEE0196, Walz GmbH, Effeltrich,

300 Germany). Samples were kept in 50 mL Greiner tubes (Thermo Fisher-Scientific, Waltham, USA) in the cold

301 (stored in a cool box on ice) and in the dark for dark-adaptation (15 min up to occasionally 4 h). Acclimation

302 times of up to 4 h did not affect photosynthetic efficiency of different phytoplankton (L. Peperzak, personal

303 communication; Eich et al., 2021). The cuvette was rinsed with ultra-pure (UP) water between samples and the

304 relative fluorescence yield (Ft) values were kept between 100 and 1000 by adjusting the PM-gain. Blanking was

305 done for each station and/or bioassay using 0.2 µm filtered seawater from the respective stations and repeated

306 after PM-gain adjustment when needed. The following formula was used to obtain the photosynthetic efficiency:

307 $F_v/F_m = (F_m-F_0)/F_m$, with F_0 being the minimum fluorescence, and F_m being the maximum fluorescence.

308

309 **2.9 Chlorophyll a concentration and pigment-based taxonomic analyses**

310 Samples (0.54 - 2.65 L) for Chl *a* concentrations and pigment-based community composition were filtered within

311 30 min of subsampling (kept on ice and in the dark) on GF/F glass fibre filters (25 mm diameter, Whatman,

312 Cytiva, Marlborough, USA) using a vacuum pump (max. 200 mbar), until filters showed clear colouring. Samples

313 were taken for total as well as a < 20 µm fraction for better compatibility with phytoplankton community

314 measurements by flow cytometry. For the < 20 µm fraction, natural seawater was reverse sieved through a 20 µm

315 mesh before filtration onto a GF/F filter. Due to low sample volume availability at bioassay A2, the same amount

316 of water from all replicates was combined for both total and < 20 µm Chl *a* samples, resulting in one averaged

317 value for each treatment. Filters were folded once and double wrapped in aluminium foil, flash-frozen in liquid

318 nitrogen and stored at -80 °C until further analysis in the home lab. Pigments were dissolved in 90 % acetone from

319 the freeze-dried filters according to Van Leeuwe et al. (2006) and high-performance liquid chromatography

320 (HPLC) pigment separation was performed (Zobrax-Eclipse XDB-C8 column, 3.5 µm particle size) according to

321 Van Heukelem & Thomas (2001). Detection of pigments was based on both the retention time and diode array

322 spectroscopy of standards (346 nm, Waters 996), quantification was based on calibration curves using those

323 standards (DHI LAB standards). Phytoplankton community composition was determined using CHEMTAX

324 version 1.95 (Mackey et al., 1996), following Selz et al. (2018). For the final pigment ratios, see Table S6.

325

326 **2.10 Phytoplankton cell abundances (< 20 µm)**

327 Phytoplankton cell abundances were obtained using a 488 nm Argon laser benchtop Beckton-Dickinson

328 FACSCalibur (BD Biosciences, Franklin Lakes, USA) flow cytometer with the trigger set on red Chl *a*

329 autofluorescence (Marie et al., 1999). The phytoplankton samples from the Amundsen Sea bioassays were

330 measured fresh within 30 min of sampling (stored on ice); the Weddell Sea bioassay phytoplankton samples were

331 fixed for 15 – 30 min with 100 µL formaldehyde-hexamine (18 % v/v:10 % v/v) at 4 °C, flash-frozen in liquid

332 nitrogen and stored at -80 °C until analysis in the home lab. Phytoplankton populations were differentiated based

333 on their red autofluorescence and side scatter, using FCS express 5 (De Novo Software, Pasadena, CA, USA).

334 Freshly counted samples resulted in comparable gating as the fixed samples (tested for Amundsen Sea samples).

A total of 25 populations were distinguished (Table S7), whereby not all populations occurred in both seas and all bioassays. Average cell diameters were determined by size-fractionation, i.e., serial gravity filtration through 20, 10, 8, 5, 3, 2, 1, 0.8 and 0.6 µm PC filters (Whatman, Cytiva, USA, Marlborough, MA) using a reuseable filter holder (Whatman, Cytiva, Marlborough, USA) and a plastic syringe. The number of cells retained by each filter per discriminated population were plotted against the respective filter size. The average cell diameters were defined as the size where 50 % of the original number of cells were retained, based on the fit of a sigmoidal plot (Veldhuis & Kraay, 2004). Phyto 5, 6, 7, 11, 12 and 14 were cryptophytes that were identified by their orange phycoerythrin autofluorescence. Based on earlier work (Biggs et al., 2019), we consider phytoplankton populations Phyto 20 and 22 to 25 to be diatoms and Phyto 8 to be *Phaeocystis antarctica* by comparing the red autofluorescence and side scatter pattern of the respective phytoplankton groups. The latter was confirmed during the Amundsen Sea expedition when we selectively collected *Phaeocystis* colonies and analysed them fresh onboard after gentle shaking (to break up the colonies). Phytoplankton carbon was estimated based on cell volume of phytoplankton, assuming spherical cells, and using 237 fg C µm^{-3} for picophytoplankton populations Phyto 1 to 6 and 196.5 fg C µm^{-3} for nanophytoplankton populations Phyto 7 to 25 (Garrison et al., 2000; Worden et al., 2004).

2.11 Statistical analyses

All statistical analyses were performed using R (R Core Team, 2021). To detect differences in phytoplankton community composition between treatments, an ANOSIM analysis was performed (vegan library, using Bray-Curtis dissimilarity with 9999 permutations). When a significant difference ($p < 0.05$) was detected, an indicator species analysis (vegan library, function r.g. with 9999 permutations) was used as a follow-up analysis to see which phytoplankton groups differed between treatments. This was done for both flow cytometry-based abundances and pigment-based taxonomic group composition, using relative values, thus normalized against total Chl *a* for pigment-based community composition, and total phytoplankton abundance for both pigment-based and flow cytometry-based phytoplankton groups. For the indicator species analysis, p-values are reported. A Scheirer-Ray-Hare test (non-parametric ANOVA-like test) was performed to determine the significance of Fe-addition and temperature increase, as well as potential interaction effects, on the respective response variable measured. The test was performed for data of the last day of the incubation, since effects were usually strongest then, and some variables were only sampled at the beginning and the end of the experiment (day 6 for A1 and A2, day 8 for W1 and W2). We manually calculated eta-squared (η^2, amount of variance explained, the higher the value, the larger

365 the effect) by dividing the sum of squares of the effect of interest (i.e. iron addition, temperature increase and the

366 interaction between these two) by the total sum of squares. The η^2 is provided when temperature increase, iron

367 addition, and/or the interaction between both tested as significant. Since we wanted to look at the overall effect of

368 Fe addition, temperature increase, and potential interaction effects on total phytoplankton abundances based on

369 flow cytometry, we additionally performed a generalized linear model (GLM), assuming a quasi-poisson

370 distribution in combination with a log-link, including the bioassay as well as the day number as factors without

371 interaction, and including an interaction term for the Fe- and temperature-treatment. For the GLM, the data of all

372 bioassays and all timepoints (excluding day 0) were combined. The formula for the GLM was: total phytoplankton

373 abundances ~ Fe treatment * temperature treatment + bioassay name + day number. Statistical results are only

374 reported for variables where more than 1 replicate was available. We also performed an NMDS analysis based on

375 phytoplankton abundances using the vegan library with Bray-Curtis dissimilarity (seed set to 123). A significance

376 level of $p < 0.05$ was used. Where applicable, the mean ± standard deviation is reported, unless stated otherwise.

377

378 **3. Results**

379 **3.1 Nutrient dynamics**

380 Bioassay treatments without Fe addition (C and T) started at naturally low dFe concentrations (0.28 ± 0.16, 0.10

381 ± 0.02, 0.05 ± 0.03 and 0.03 ± 0.01 nM natural dFe for bioassay A1, A2, W1 and W2, respectively), and stayed

382 within these ranges. The Fe addition treatments (F and TF) showed a rapid (and overall comparable) drawdown

383 of the added Fe (natural Fe for A1 and A2; Fig 2a, b and d^{57}Fe for W1 and W2; Fig. 2e, f) in all bioassays,

384 regardless of its isotopic composition. The dFe concentrations in F and TF treatments (0.29 ± 0.07 nM) at the end

385 of the bioassays were comparable to concentrations in non-Fe addition treatments (0.28 ± 0.14 nM) for the

386 relatively high-Chl *a* bioassay A1. In contrast, bioassay A2 had most dFe left at the end of the incubation (0.80 ±

387 0.46 nM for F and TF, compared to 0.11 ± 0.04 nM for C and T) which concurs with the low starting Chl *a*

388 concentration and irradiance intensity. However, since the average dFe concentration in Fe amended treatments

389 was lower (0.65 ± 0.10 nM) in the middle of the incubation period (day 3, see Figure 2 b), we cannot rule out

390 potential contamination during sampling as a reason for the higher dFe concentrations, notably in the F treatment.

391 For the Weddell Sea bioassays, d^{57}Fe in F and TF treatments declined rapidly with low final concentrations (0.14

392 ± 0.03 and 0.31 ± 0.17 nM for W1 and W2, respectively) compared to the non-Fe addition treatments (0.01 ± 0.01

393 nM d^{57}Fe and below detection limit for W1 and W2, respectively). Other trace metals were also measured, and

394 dissolved manganese (dMn) drawdown did not differ between treatments (Fig. 2g-j). However, the starting

395 concentrations of dMn were low for W1 and W2 (0.06 ± 0.03 and 0.19, SD < 0.01 nM, compared to 0.76, SD <

396 0.01 1.16 ± 0.01 nM for A1 and A2, respectively).

397 The dissolved inorganic macronutrients were not limiting phytoplankton growth during the bioassays. Final

398 concentrations were at least 7.2, 0.3 and 37 µM in all bioassays for nitrogen, phosphate, and silicate, respectively

399 (Supplement Fig. S2). Still, there was discernible drawdown of macronutrients by the microbial community during

400 the incubations, except for Amundsen Sea bioassay A2. Fe addition (both F and TF treatments) had a significant

401 impact on phosphorous drawdown for bioassays A1, W1 and W2 ($p < 0.05$, η^2: 0.53, 0.76 and 0.76 for A1, W1

402 and W2, respectively; and on average 0.45 µM lower for Fe addition treatments compared to C) and on nitrogen

403 drawdown for bioassays W1 and W2 ($p < 0.004$, $\eta^2 > 0.75$, average of 9.8 µM lower for Fe addition treatments

404 compared to C). The TF treatment showed stronger drawdowns especially for Weddell Sea bioassays W1 and W2

405 (average 0.7-fold change between TF and F treatments for both phosphorus and nitrogen, respectively), however

406 there was no significant interaction effect between temperature increase and Fe addition. In contrast, silicate acid

407 concentrations at the end of the incubation period were impacted by the increase in temperature for bioassays A1,

408 A2 and W2 ($p < 0.02$, η^2: 0.76 for A1 and W2 and η^2: 0.52 for A2 and $p = 0.06$ and η^2: 0.32 for bioassay W1),

409 with T treatments showing on average a 2.4 µM lower silicate concentration compared to the control. Only

410 bioassay W1 showed an effect of Fe-addition on silicate drawdown ($p = 0.02$, η^2: 0.52), resulting in the TF

411 treatment showing lowest concentrations on the last day of the incubations (0.8-fold change compared to the

412 control and 0.9-fold change compared to both T and F treatment). The ratios of silicate drawdown to nitrogen and

413 to phosphorus were higher in W1 than in W2 (i.e., 1.4 and 18.3 in W1 and 0.7 and 10.5 in W2). Moreover, when

414 Fe was added, the silicate to nitrogen ratio (Si:N), as well as silicate to phosphorous ratio (Si:P) drawdown was

415 lower in bioassays A1, W1 and W2 compared to non-Fe treatments (0.86 and 1.02 Si:N for Fe and non-Fe

416 treatments and 11.3 and 12.5 Si:P, respectively).

417
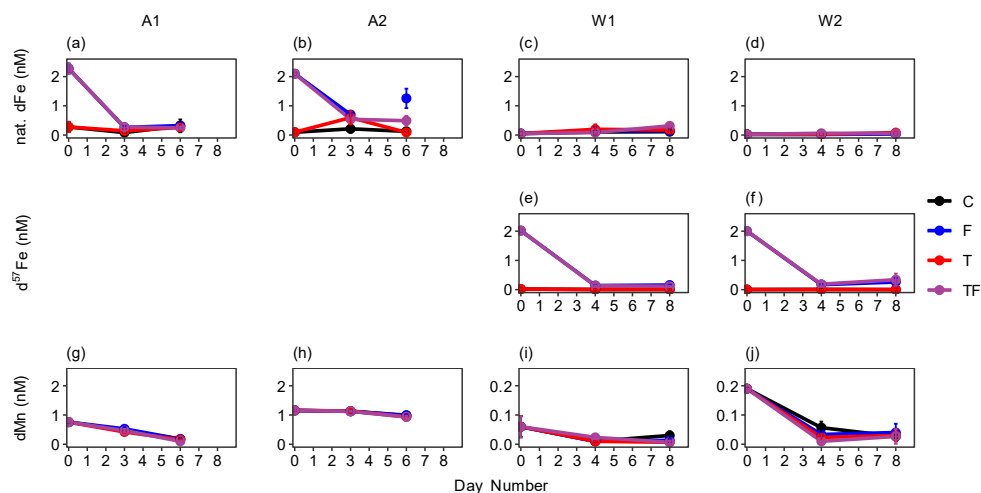
Figure 2: Average concentrations of natural dissolved Fe (a, b, c, d), d^{57}Fe (e, f) and dMn(g, h, i, j) concentrations for Amundsen Sea (A1: a, g; A2: b, h) and Weddell Sea (W1: c, e, i; W2: d, f, g) bioassays. Amundsen Sea bioassays did not receive 57Fe supplementation. The black line represents the control (C) treatment, the red line the temperature (T) treatment, the blue line the iron (F) treatment, and the purple line the combined temperature and iron treatment (TF). Error bars indicates the standard deviation (n = 2 or 3, except for dFe of bioassay A2 TF treatment day 3, when they are not visible it is smaller than the symbol. Bioassay A2 showed a higher dFe concentration on day 6 compared to day 3, which we cannot exclude to be due to potential contamination and was thus treated as an outlier.

Particulate Fe concentrations (natural pFe for A1, p^{57}Fe for W1 and W2) increased over time for the Fe addition treatments (Table S8) in all bioassays examined (excluding A2 as particulate metals were not measured there), and pFe concentrations at the last day of incubations were (positively) impacted by Fe-addition (p ≤ 0.01, η^2 ≥ 0.73 for A1, W1 and W2, final concentrations were 8.01 ± 0.83, 1.09 ± 0.10, 0.89 ± 0.33 nM for Fe addition treatments and 4.40 ± 0.21, 0.08 ± 0.02, 0.09, SD < 0.01 nM for treatments without Fe addition for A1, W1 and W2, respectively).

To examine potential differences in phytoplankton trace metal stoichiometry in response to Fe addition and/or warming, we calculated the ratio of pFe and other trace metals (pMn, pZn, pCd and pCu) to POP concentrations (Fig. 3, Table S8). Fe-addition significantly increased pFe:POP ratios (natural pFe for A1 and p^{57}Fe for W1, W2) for all bioassays (p ≤ 0.01, η2 ≥ 0.73; average 2.5-fold change for natural pFe:POP (A1) and 13.3-fold change for p^{57}Fe:POP in Weddell Sea bioassays for Fe-addition treatments compared to the control). Furthermore, the pMn:POP ratios increased (by 0.33 compared to C) due to Fe-addition in bioassay A1 and decreased (by 0.13 compared to C) in W2 (p < 0.01 and 0.004, η2: 0.74 and 0.76, respectively). For bioassay W1, neither Fe nor temperature alone had a significant impact on the pMn:POP ratio, however, the combination of both treatments tested significant (p = 0.01, η2: 0.63), with the TF treatment showing an average 1.4-fold changed ratio compared to all other treatments. Also, the pCd:POP ratio was significantly affected by Fe-addition in W1 and W2 (p < 0.05,

443   η2: 0.76 and 0.39 for W1 and W2), showing decreased values (by on average 0.12) for Fe-addition treatments

444   compared to the control (Fig. 3 o-q), however no effect was seen for bioassay A1. A similar outcome was observed

445   for pZn:POP ratios (p ≤ 0.01, η2: 0.65 and 0.76 for W1 and W2, respectively, by on average 1.8 compared to C).

446   For pCu:POP ratios, a decrease due to Fe-addition was mainly observed in bioassay A1 and W2 (p < 0.009, η2 ≥

447   0.73, by on average 0.16 compared to C), while for bioassay W1, Fe-addition caused a notable, but not statistically

448   significant effect (p = 0.09, η2: 0.32, Fig. 3, by on average 0.23 compared to C).

449
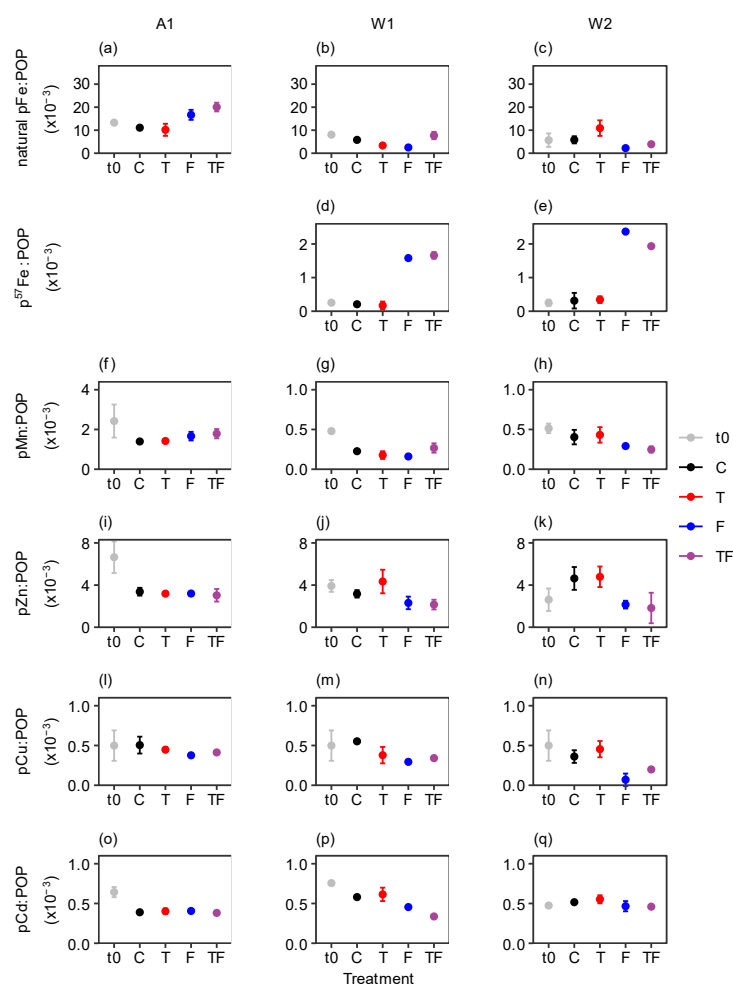
Figure 3: Average ratios (x10^{-3}, mM:M) of particulate trace metal to particulate organic phosphorus (POP) for Amundsen Sea A1 (a, f, I, l, o) and Weddell Sea W1 (b, d, g, j, m, p) and W2 (c, e, h, k, n, q) bioassays. There is no data available for A2. pFe = natural particulate, p^{57}Fe = particulate iron in the ^{57}Fe form (not added to Bioassay A1), pMn = particulate Manganese, pZn = particulate Zinc, pCu = particulate copper, pCd = particulate cadmium. t0 are starting ratios, whilst ratios for C (control), T (temperature), F (iron) and TF (combination of temperature and iron) were measured on the last day of the incubations (day 6 and 8 for Amundsen and Weddell Sea bioassays, respectively). Error bars indicates the standard deviation (n = 2 or 3), except for bioassay A1, T-treatment for all ratios and bioassay W1 C treatment for the pFe:POP ratio, there n = 1. If the error bar is not visible, then it is smaller than the symbol. Please note the different y-axis ranges for manganese to POP ratios (f–h).

3.2 Photosynthetic efficiency

459

460   The photosynthetic efficiency F_v/F_m at the start of the incubations was 2-fold lower for the Weddell Sea bioassays

461   compared to the Amundsen Sea bioassays (i.e., 0.3 *vs* 0.6 r.u., respectively). Fe addition led to an increase of

462   F_v/F_m for all bioassays (Fig. 4, $p \leq 0.009$; $\eta^2 > 0.68$ for all bioassays), with stronger increases in Weddell Sea

463   compared to Amundsen Sea bioassays (average of 1.42- and 1.14-fold change for Fe addition (F and TF) versus

464   control treatments for Weddell and Amundsen Sea bioassays, respectively). Towards the end of the incubations

465   of W1 and W2, F_v/F_m decreased slightly again for the Fe addition treatments (most so for TF, with final F_v/F_m

466   values being still higher than for C and T treatments), coinciding with Fe depletion (Fig. 2).

467
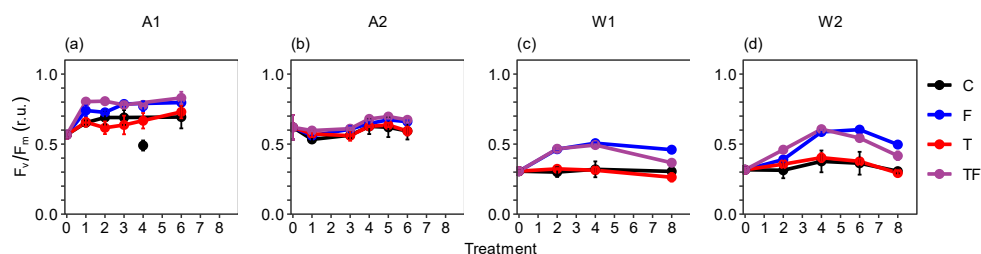
468

469   **Figure 4:** Temporal dynamics of the photosynthetic efficiency (F_v/F_m, relative units) of the phytoplankton for the Amundsen
470   Sea A1 (A), A2 (B) and the Weddell Sea W1 (C) and W2 (D) bioassays. The black line represents the control (C) treatment,
471   the red line the temperature (T) treatment, the blue line the iron (F) treatment, and the purple line the combined temperature
472   and iron (TF) treatment. Averages of triplicates with error bars representing the standard deviation; if not visible it is smaller
473   than the symbol. The control treatment of bioassay A1 showed an outlier for F_v/F_m values on day 4, which was excluded.

474

3.3 POC, Chl *a*, and phytoplankton taxonomic community composition

475

476   Total Chl *a* concentration at the start of the incubations (Table 1) was highest for the ASP bioassay A1 (3 µg L^{-1})

477   and lowest for bioassay A2 outside the ASP (0.4 µg L^{-1}). Of the Weddell Sea bioassays, W1 had the highest Chl

478   *a* starting concentration (1.5 compared to 0.6 ug L^{-1} for W1 and W2). Starting concentrations of total POC in A1

479   and W1 were higher than A2 and W2 (384 and 347 ug L^{-1} compared to 91 and 136 ug L^{-1}, respectively). The POC

480   to Chl *a* ratio was lower for A1 (130) than the other bioassays (212-239). Total POC concentrations did not display

481   differences between treatments at the end of the incubations for A1 and A2 (Fig. 5a-d), yet total Chl *a*

482   concentrations exhibited treatment-specific differences for all bioassays (Fig. 5e-h). Fe-addition always positively

483   impacted Chl *a* concentrations (p: 0.02, 0.005 and 0.006, η^2: 0.52, 0.76 and 0.67 for bioassays A1, W1 and W2;

484   not tested for A2 due to n = 1 for all Chl *a* samples and W1 C due to n = 1), however the effect was stronger in

485   Weddell Sea Bioassays (average of 1.6- and 2.9-fold difference for Amundsen and Weddell Sea with Fe addition

486   compared to C). Amundsen Sea bioassays also showed a slight increase in Chl *a* with increased temperatures.

487   Strongest treatment-specific increases in Chl *a* concentrations were, however, obtained for the TF treatment in all

488   bioassays, resulting in an average of 1.7 µg more Chl *a* L^{-1} compared to the F treatment. POC concentrations in

489   W1 and W2 showed similar treatment responses as total Chl *a* in these bioassays.

490   The TF treatment also caused the strongest increase for the < 20 µm Chl *a* fraction (Fig. 5 e–h) for all bioassays,

491   and Fe-addition generally had a positive impact on < 20 µm Chl *a* concentrations, with effects being strongest in

492   both Weddell Sea bioassay W1 and W2 (increases of 1.2, 0.2, 0.5 and 0.7 µg L^{-1} for A1, A2, W1 and W2 compared

493   to the control, respectively and p = 0.04 and 0.006, η^2: 0.37 and 0.67. A2 and W1 were not tested due to missing

494   replicates). The < 20 µm fraction at the start of the bioassays made up respectively 42, 24 and 65 % of total Chl *a*

495   in A1, W1 and W2, whereas for bioassay A2 95 % of the total Chl *a* concentration was < 20 µm. At the end of

496   the bioassays, shares were 42, 25, 35 % and 70 % for A1, W1, W2 and A2, respectively.

497   Diatoms dominated the phytoplankton community at the start of A1 and W1 (53 and 62 % of total Chl *a*), followed

498   by haptophytes (34 and 27 %; Fig. 5i-l). Bioassay W2 had a comparable share of diatoms and haptophytes (42

499   and 46 % of total Chl *a*), whilst the phytoplankton community of A2 was taxonomically most diverse.

500   Diatoms showed in general a strong response to Fe addition (F and TF treatment) and could be defined as an

501   indicator group for Fe addition treatments in A1 and W2 (p < 0.005). Absolute diatom abundances increased as

502   well with Fe-addition, especially for the TF treatment, in bioassays A1 (F and TF treatment, p = 0.007) and W2

503   (TF treatment, p = 0.02, Table S8). In bioassay W2, diatoms also showed a higher share for Fe addition treatments

504   in the < 20 µm fraction (p < 0.05), with absolute abundances being higher in the TF treatment for bioassays A1,

505   W1 and W2 (p < 0.04), and bioassay W1 also showing higher abundances at the F treatment (p = 0.04). The

506   contribution of haptophytes declined (in response to the diatom increase, also in W1 where the diatom response

507   was not significant, p < 0.007), however their absolute concentration (in µg Chl *a* L^{-1}; Table S8) did not decline

508   except for the F-treatment in bioassay W2 (p = 0.01). Both the share (p = 0.01) and absolute concentration (p =

509   0.04) of pelagophytes increased with Fe addition in the < 20 µm fraction of bioassay A1. Cryptophyte abundances

510   increased in the total fraction of the TF treatment for A1 and W2 (p = 0.02 and 0.01, respectively), and the < 20

511   µm fraction in W1 (p = 0.02), however their share did not change with treatments.

512
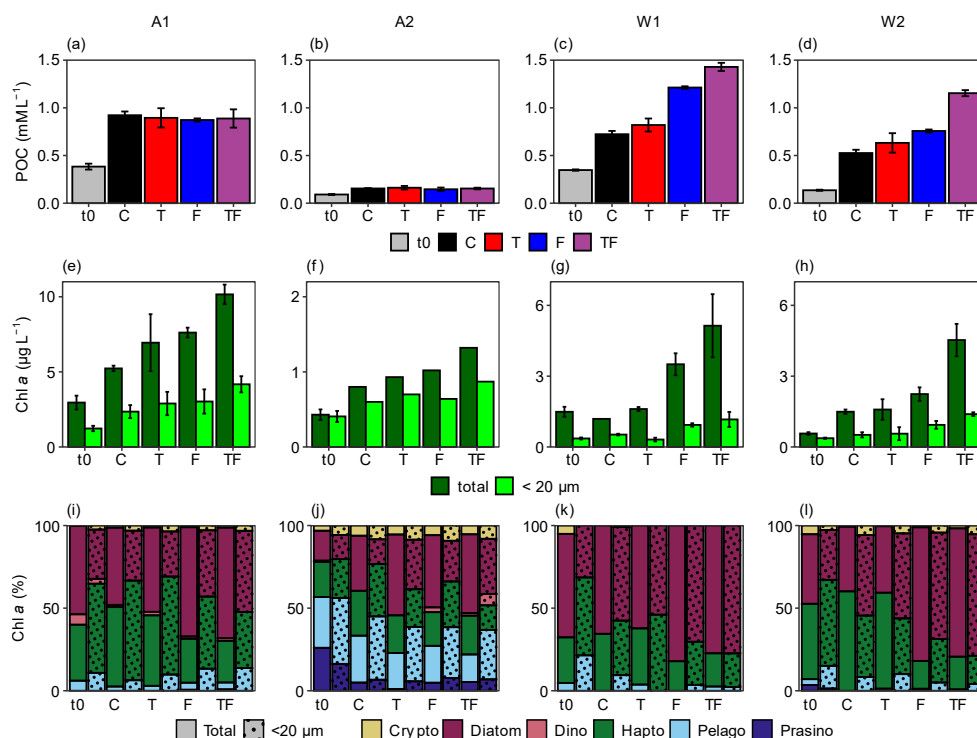
Figure 5: Average concentrations of particulate organic carbon (POC, a-d), total and < 20 µm (dotted columns) Chl *a* (e-h), and the taxonomic composition of the phytoplankton community (i-l , % of total Chl *a*) for the Amundsen Sea A1 (a, e, i) and A2 (b, f, j), and the Weddell Sea W1 (c, g, k) and W2 (d, h, l) bioassays. Error bars represent the standard deviation (n = 3 except when no error bar is shown, then n = 1). t0 = starting conditions, C = control, T = temperature treatment, F = iron addition treatment, TF = temperature and iron addition treatment. For i-l, Crypto, Dino, Hapto, Pelago and Chloro stands for cryptophytes, dinophytes, haptophytes, pelagophytes and chlorophytes, respectively. Solid bars represent the total and shaded bars the < 20 µm fraction community composition. Note the difference in y-axis for the Chl *a* panels e-h.

520

3.4 Phytoplankton abundances

522   The total abundances of < 20 µm phytoplankton (Fig. 6, Fig. S3, Table S8) increased with time for all bioassays

523   and the treatment-specific dynamics largely mimicked the responses observed for the < 20 µm Chl *a* fraction (Fig.

524   5e-h). Bioassay A1 had overall the highest phytoplankton abundances (up to 40,000 ± 4,000 cells mL^{-1} for the TF

525   treatment; Fig. 6a) and was dominated by *Phaeocystis antarctica* Phyto 8 (highest abundances of 37,053 mL^{-1}

526   were observed in the TF treatment; Table S8). Phyto 19 increased specifically in abundance and share (Fig. 6a) in

527   the temperature treatments (2,800 and 3.500 cells mL^{-1} for T and TF, compared to 1,700 and 1.300 mL^{-1} for C and

528   F, p < 0.01). Phyto 24 was positively impacted by the TF treatment, i.e., 361 *vs* 595 cells mL^{-1} for C and TF

529   treatment, respectively (p < 0.05).

530
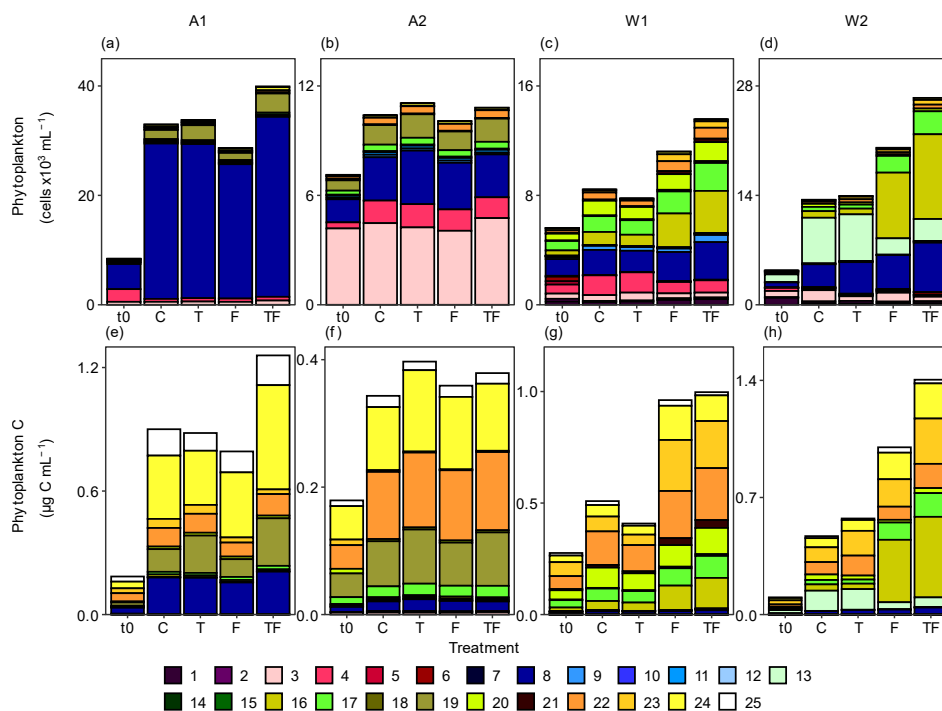
Figure 6: Flow cytometry-based phytoplankton community composition (a-d) and carbon (e-h) at the start (t0) and the end
of the bioassay incubations for the different treatments (average of triplicates) for Amundsen Sea bioassays A1 (a, e), A2 (b,
f), and Weddell Sea bioassays W1 (c, g) and W2 (d, h). t0 = starting conditions, C = control, T = temperature treatment, F =
iron addition treatment, TF = temperature and iron addition treatment. Phytoplankton groups are sorted by size, with Phyto 1
– 6 ≤ 3 µm, Phyto 7 – 20 ≤ 10 µm and Phyto 21 – 25 ≥ 10 µm. Phyto 5, 6, 7, 11, 12 and 14 are cryptophytes, Phyto 20, 22 –
25 diatoms and Phyto 8 *Phaeocystis antarctica*. Note the different scales.

537

When converted to cellular carbon based on cell volume using 237 and 196.5 fg C µm^{-3} as conversion factors for

Pico- and Nanophytoplankton, respectively (Fig. 6e), the strong positive response of the phytoplankton to the TF

treatment was mostly due to this larger-sized Phyto 24 (average diameter of 19 µm, p = 0.01, stat: 0.92) and to

smaller extent Phyto 19 (p < 0.01). Bioassay A2 presented the highest share of picoeukaryotes, especially Phyto

3 (59 % compared to max. 18 % in the other bioassays, Fig. 6b). No apparent treatment-specific responses were

recorded, apart from Phyto 19 that increased somewhat with warming (p = 0.04). The phytoplankton populations

in W1 were distributed more equally (Fig. 6c), with higher abundances of especially Phyto 16 and 17 for the Fe

addition treatments (p < 0.05, most pronounced for TF with average abundances of 3,103 ± 1,290 *vs* 948 ± 218

cells mL^{-1} and 2,041 ±572 *vs* 1,158 ± 216 cells mL^{-1} for Phyto 16 and 17 in the TF *vs* C treatments, respectively).

When expressed in carbon, Phyto 16 was still a recognisable indicator species (p = 0.03) but at the same time the

larger-sized Phyto 21 (average cell diameter of 10 um) and diatoms Phyto 22-24 (13-19 µm) showed clear positive

responses to Fe addition (Fig. 6g, p < 0.05 for all). Bioassay W2 also showed a distinct shift in favour of Phyto

550   16 and Phyto 17 (away from Phyto 13), already early in time (Table S8), both for abundances and cellular carbon

551   (Fig. 16d, h, p < 0.01 for all). Diatom 24 responded positively to Fe addition (F and TF, Fig. 16h, p < 0.01), similar

552   as for bioassay W1, and diatom Phyto 23 showed higher abundances for the TF treatment (p = 0.04). Phyto 19

553   was the only phytoplankton population that showed a consistent selective positive response (in share) to warming

554   (and not to Fe addition) in the Amundsen Sea bioassays. Diatom Phyto 22 increased with temperature in bioassay

555   W2 (p ≤ 0.01). We refer to Table S8 for less pronounced responses of the other phytoplankton populations.

556   Overall, the response by the larger phytoplankton populations is also illustrated by the higher average cellular

557   biovolumes in the F and TF treatments of W1 and W2 (Fig. S4). The Amundsen Sea bioassays did not show a

558   treatment-specific increase in phytoplankton biovolume. Fe-addition had a significant effect on total

559   phytoplankton abundances for Weddell Sea bioassays (p < 0.02, η^2: 0.96 and 0.74 for W1 and W2, with Fe addition

560   leading to an average 1.6-fold change compared to C). The GLM we performed (explained deviance: 86 %),

561   indicates an interaction effect of Fe-addition and warming (p = 0.03 for the interaction, exponentiated coefficient

562   (ec): 1.13), i.e. Fe-addition of 2 nM in combination with a 2 °C temperature increase led to an overall increase in

563   algal abundances of about 28 %. Fe-addition (ec: 1.03), temperature increase (ec: 1.11), bioassay and day number

564   (p < 0.001 for all, for other statistical parameters, see Table S9) were also significant explanatory factors. The

565   NMDS analysis of the Weddell Sea bioassays (Fig. S5c, d) demonstrated clear distinction between the Fe addition

566   treatments and the non-addition treatments after the second day of the incubations. For bioassay W1, the TF and

567   T treatments clustered on the last day of incubation separately from the F and C treatments, respectively. For

568   bioassay W2, the T treatment also separated on the last day while the TF and F treatments remained closer

569   together. Bioassays A1 and A2 did not display obvious clustering by treatment, other than time (i.e., separation

570   after day 2).

571

572   **4. Discussion**

573   **4.1 Trace metal and macronutrient dynamics**

574   The pFe concentrations showed the expected significant increase in the Fe addition treatments for both Amundsen

575   (natural dFe added) and the Weddell Sea bioassays (d^{57}Fe added) at both temperatures, indicating that the added

576   dFe was indeed taken up and incorporated in the phytoplankton cells. Additionally, in bioassay W2 the final p^{57}Fe

577   in the TF treatment was higher than in the F treatment (1.12 ± 0.11 nM compared to 0.66 ± 0.20 nM),

578   demonstrating enhanced Fe uptake with higher temperatures. The higher starting concentrations of dFe in the

579   Amundsen Sea, compared to the Weddell Sea, can be attributed to the Fe input from basal melt (Rignot et al.,

580   2013). Conversely, the naturally low dFe concentrations in the Weddell Sea underscore the area's limited Fe input

581   (e.g. de Baar et al., 1990; Klunder et al., 2012).

582   Fe is needed in nitrate assimilation and as such uptake of nitrate is coupled to the Fe nutritional status (Schoffman

583   et al., 2016). Similarly, diatom cellular silicate to nitrogen ratios are known to increase in response to Fe stress

584   (Meyerink et al., 2017). Highest drawdown of the macronutrients typically occurred in the TF treatment, which

585   also showed the largest phytoplankton accumulation. However, whilst dissolved inorganic phosphate and nitrogen

586   drawdown was mostly affected by Fe addition, silicate drawdown in bioassays A1 and W2 was more impacted by

587   temperature. Despite a lower Chl a concentration (both total and < 20 µm) and phytoplankton abundance for the

588   T than the TF treatment in these bioassays, the silicate drawdown was comparable. Although Fe stress is reported

589   to cause reduced cellular Chl a concentrations compared to Fe replete conditions (Greene et al., 1992), it is an

590   unlikely cause as the total phytoplankton abundances displayed similar differences between the T and TF

591   treatment compared to < 20 µm Chl a concentrations. Instead, higher temperature may have stimulated Si uptake,

592   as reported for the diatom *Pseudonitszchia seriata* at temperatures above 0 °C (Stapleford & Smith, 1996). It

593   might also be that the T treatment experienced higher Fe stress than the control, which is also known to increase

594   Si uptake (Meyerink et al., 2017). However, since phytoplankton abundances and Chl a concentrations were not

595   higher in T treatments compared to the control, and since phytoplankton requires less Fe at higher temperatures

596   (Jabre & Bertrand, 2020), this is less likely. Bioassay W1 showed the strongest decline in silicate concentrations,

597   with both temperature and Fe affecting silicate drawdown. The relatively high fraction of diatoms (and specifically

598   the large-sized Phyto 20 and 22-24) in bioassay W1 could theoretically have caused the strong silicate drawdown

599   and high ratio of silicate relative to nitrogen (or phosphorus) uptake for all treatments. However, A1 also had high

600   diatom abundances and over the course of the incubations the concentration of diatoms in W2 became comparable

601   to W1. An alternative explanation may be that Mn stress in W1 (0.06 ± 0.04 *vs* 0.19 ± 0 nM in W1 and W2,

602   respectively) enhanced Si uptake, similar to Fe stress (Hutchins & Bruland, 1998). Increased Si uptake by diatoms

603   under a combined Fe and Mn limitation may possibly enhance protection against grazers (Assmy et al., 2013;

604   Ryderheim et al., 2022) and/or enhance sinking to more nutrient-rich depths (Waite & Nodder, 2001). Considering

605   an increasing awareness of trace metal co-limitation of phytoplankton growth (Wu et al., 2019; Browning et al.,

606   2021; Balaguer et al., 2022; Burns et al., 2023), we recommend further investigation into these potential

607   interactions and their ecological relevance.

608   Dissolved Mn is known to (co-)limit Southern Ocean phytoplankton growth and community composition

609   (Balaguer et al., 2022). Although Fe addition (F and TF treatments) led to 1.8 (0.11 ± 0.03 *vs* 0.06 ± 0.02 d^{-1}) and

610 1.5-fold (0.23 ± 0.02 *vs* 0.15 ± 0.01 d^{-1}) higher net growth rates (based on total phytoplankton abundances) in W1

611 and W2 compared to the control. The lower starting concentrations of dMn in W1 compared to W2 may have

612 contributed to the 2-fold lower phytoplankton net growth rates in W1 compared to W2, independent of the

613 treatment. Since Fe addition still led to an increased growth rate even with low dMn concentrations, Fe must have

614 been the main limiting factor.

615

616 **4.2 Micronutrient stoichiometry**

617 The observed pFe:POP ratios increased upon the addition of iron (natural pFe for bioassay A1 and p^{57}Fe for

618 bioassays W1 and W2), validating the experimental design and confirming the uptake of added dFe by

619 phytoplankton. For other bio-essential (Mn, Zn, Cu) or bio-active (Cd) metals, the metal:POP ratio is expected to

620 be elevated under Fe stress due to upregulation of non-specific divalent metal transporters under Fe stress (e.g.

621 Kustka et al., 2007; Lane et al., 2008) or the increased uptake of phosphorous relative to metals under Fe replete

622 conditions (growth-dilution; Cullen et al., 2003). Specifically for Mn, this might also be due to a higher cellular

623 Mn requirement under Fe stress (Peers & Price, 2004). The pMn:POP ratios were indeed higher in the C and T

624 treatments compared to the F and TF treatments of W2, but for W1, no consistent effect of Fe was observed (Fig.

625 3).

626 In contrast, slightly elevated pMn:POP ratios were observed after Fe addition in A1 (F and TF treatments),

627 matching findings by McCain et al. (2021) and Hawco et al. (2022), showing increased Mn demand in

628 environments with high Fe concentrations. Such variation likely reflects adaptive changes in nutrient uptake and

629 storage mechanisms under nutrient stress but could also be due to different phytoplankton community

630 compositions and/or environmental conditions. For example, Twining et al. (2004) observed elevated pMn:POP

631 ratios in individual diatom cells under iron deplete conditions, relative to iron replete conditions, whereas the trend

632 was opposite for autotrophic flagellated cells. However, diatoms were dominant in the F and TF treatments in all

633 experiments, suggesting that other factors besides differences in community composition play a role. The starting

634 dMn concentrations differed between the bioassays, whereby the high starting concentrations of dMn in A1 could

635 potentially explain the increased pMn:POP ratios in the F and TF treatments of this experiment., We speculate

636 that a high availability of both Fe and Mn under the low light conditions in A1 could have led to increased Mn

637 uptake for use in photosynthesis. Since dMn levels are thought to increase with Fe input (e.g. due to ice shelf

638 melting; Van Manen et al., 2022), we recommend including dMn in future studies examining the effects of global

639 climate change on phytoplankton growth.

640   Besides Mn, other trace metals are known to have variable ratios with respect to POP under different

641   environmental conditions. For example, cellular Cu requirements increase under Fe limitation (Schoffman et al.,

642   2016), which could explain the higher pCu:POP ratios in the C and T treatments compared to the Fe addition

643   treatments (Fig. 3). Similarly, the pZn:POP ratios were also elevated in the non-Fe treatments in W1 and W2, akin

644   to the pCd:POP ratios especially in W1, suggesting higher uptake of metals under Fe limitation as previously

645   suggested (Cunningham & John, 2017). Future studies linking these stoichiometric ratios with molecular

646   measurements (e.g. protein expression patterns) could provide further insight into the processes which underpin

647   trace metal uptake and use within phytoplankton communities under change. Nevertheless, this study highlights

648   a potential trend of increased uptake of essential and non-essential metals (specifically zinc, copper and cadmium)

649   by phytoplankton under Fe-deplete conditions. This trend underscores the adaptive strategies employed by

650   phytoplankton in navigating nutrient scarcities, emphasizing the complexity of nutrient interactions and their

651   collective impact on phytoplankton ecology under varying environmental conditions (e.g. Cunningham and John,

652   2017). Due to the importance of nutrient uptake in the Southern Ocean for the stoichiometry of global nutrient

653   distributions, notably at lower latitudes (Sarmiento et al., 2004; Middag et al., 2020), changes in (micro-)nutrient

654   consumption in the Southern Ocean can have global ramifications for both productivity and ecosystem structure

655   (Moore et al., 2018) which should be further explored in future (modelling) studies.

656

657   4.3 Impact of Iron and Temperature on Phytoplankton Dynamics

658   The Weddell Sea bioassays exhibited stronger Chl *a* accumulation and increased phytoplankton abundances in

659   response to Fe addition than the Amundsen Sea bioassays, which is likely due to the lower dFe concentrations

660   (and hence higher degree of Fe limitation for the phytoplankton typical for the Weddell Sea) at the start of the

661   incubations. While for the Weddell Sea bioassays the POC concentrations followed comparable responses to total

662   Chl *a* upon Fe addition (Fig. 5), the POC concentrations in the Amundsen Sea bioassays did not. The lower

663   irradiance during the incubations of A1 and A2 most likely led to the higher Chl *a*:POC ratios at the end of

664   incubations (i.e., average over all treatments 0.008 ± 0.002 and 0.003 ± 0.003 for the Amundsen and Weddell Sea

665   bioassays). Enhanced Chl *a*:POC ratios are a known acclimation to low light (Laws & Bannister, 1980; Geider,

666   1987; Geider et al., 1998; Wang et al., 2009). Despite the low light intensities, Chl *a* concentrations and

667   phytoplankton abundances in the control treatment increased over time in the Amundsen Sea bioassays (especially

668   in A1, net growth rate based on abundances of 0.23 ± 0.02 d^{-1}), which indicates that the phytoplankton

669   communities were low light adapted. Low light conditions are common for Amundsen Sea phytoplankton

670   (Schofield et al., 2015; Park et al., 2017) but still, the very low irradiance in A2 seemed to have limited growth

671   (0.09 ± 0.01 d^{-1}) as also illustrated by incomplete depletion of the dFe added (after 6 days of incubation). Although

672   earlier studies reported positive responses of phytoplankton to Fe addition also under low light conditions (Viljoen

673   et al., 2018; Alderkamp et al., 2019), the light intensities used for the low light treatment in those studies were

674   relatively high (i.e., 15 and 30 µmol quanta m^{-2} s^{-1}) and well above those in A1 and A2 (average of 3.4 and 1.5

675   µmol quanta m^{-2} s^{-1}). Considering diatoms being the taxonomic group responding strongest to Fe additions (Noiri

676   et al., 2005; Feng et al., 2010; Hinz et al., 2012; Mills et al., 2012; Zhu et al., 2016), the low proportion of diatoms

677   at the start of A2 may also have delayed a measurable effect of Fe addition. Since both Weddell Sea and Amundsen

678   Sea bioassays were initiated at times corresponding to the peak phytoplankton growth periods in each region, it is

679   unlikely that the sampling time had a major effect on our results.

680   Consistent with the lower dFe concentrations was the reduced *in-situ* F_v/F_m of the phytoplankton in W1 and W2

681   compared to Amundsen Sea bioassays, which stayed low for non-Fe addition treatments throughout the

682   experiments. Although we cannot exclude that the lower light availability in A1 and A2 may have caused

683   enhanced F_v/F_m (compared to W1 and W2; From et al., 2014), low F_v/F_m is a common indicator of Fe stress in the

684   Southern Ocean (Greene et al., 1992; Olson et al., 2000; Mills et al., 2012; Jabre and Bertrand, 2020). In addition,

685   the low dMn concentration at the start of bioassay W1 may have contributed to the low F_v/F_m (Wu et al., 2019).

686   Nevertheless, Fe addition also had a positive effect on F_v/F_m in Amundsen Sea bioassays, matching earlier reports

687   that F_v/F_m of ASP phytoplankton is partly controlled by Fe (Alderkamp et al., 2015). The decrease in F_v/F_m in the

688   F and TF treatments towards the end of the Weddell Sea bioassays might indicate that added Fe depleted towards

689   potentially limiting conditions or might be an indication of Mn (co-)limitation.

690

4. 4 Enhanced responses to Fe with warming

692   Fe addition led to an overall positive response of Chl *a* concentrations, phytoplankton photophysiology and

693   growth, but more so when combined with the ecologically relevant increase in temperature. The increase in

694   phytoplankton abundances was especially distinct for Weddell Sea bioassays. GLM analysis revealed that

695   temperature alone was a significant factor for total phytoplankton abundances, however more specifically, only

696   Phyto 19 and Phyto 22 abundances displayed significant positive responses to temperature alone (T treatment).

697   The 2 °C warming alone was thus not a major driver of phytoplankton net growth in our bioassays, but accelerated

698   and enhanced Fe-addition responses (significant interaction effect for iron addition and temperature increase on

699   total phytoplankton abundances). The enhanced response to Fe with temperature was especially distinct for

700   bioassay W2 (average 1.61-fold change in the TF treatment compared to both F and T treatments). Despite low

701   light levels, this was also seen in Amundsen Sea bioassay A1, albeit to a lower extent (average 1.29-fold change

702   in the TF treatment compared to both F and T treatments). Larger-sized (> 20 µm) diatoms were mainly

703   responsible for the Chl *a* accumulation, which is consistent with previous studies (Noiri et al., 2005; Feng et al.,

704   2010; Hinz et al., 2012; Mills et al., 2012; Zhu et al., 2016) and supports the general consensus that especially

705   large phytoplankton show enhanced growth upon Fe addition due to their lower surface to volume ratio (Scharek

706   et al., 1997). But also (slightly) smaller diatoms Phyto 23 and 24 (average cell diameter of 15 and 19 µm,

707   respectively) responded positively to the combination of Fe and temperature. Diatoms Phyto 24 was even the main

708   phytoplankton population responsible for the increase in the < 20 µm Chl *a* fraction of the TF treatment in A1.

709   The NMDS analysis based on < 20 µm phytoplankton abundances showed clustering for W1 and W2 driven by

710   Fe addition and temperature, indicating that also smaller-sized phytoplankton display positive responses. This is

711   supported by increased < 20 µm Chl *a* concentrations and the 2.2 fold change in cellular carbon of < 20 µm

712   phytoplankton in F and TF treatments in the Weddell Sea bioassays (compared to the C and T treatments).

713   Specifically, we recorded distinct abundance increases of the small 7 µm Phyto 16 and Phyto 17, in the F and TF

714   treatments of W2. *Phaeocytis antarctica* (Phyto 8; 3.7 µm) also displayed higher abundances under the TF

715   treatment for W2 but the effect was not very apparent and overall, *P. antarctica* seems to handle the other

716   treatments consistently well. Rose et al. (2009) and Zhu et al. (2016) also found diatoms preferentially stimulated

717   by Fe addition and/or temperature over *P. antarctica*, which was also found in a broader context where *P.*

718   *antarctica* dominated under Fe-low conditions, whilst diatoms dominated in regions with higher Fe concentrations

719   (Arrigo et al., 2017). In contrast, Andrew et al. (2019) found comparable growth rates for *P. antarctica* and several

720   diatom cultures (tested under Fe addition and warming treatments). Similar to our study, they found highest

721   growth for the combined Fe addition and warming treatment for most species. Since diatoms tended to increase

722   strongest with Fe addition, it can be speculated that phytoplankton community compositions shift towards more

723   diatoms with increases in Fe concentrations, however other biogeochemical factors are also important to consider.

724   The positive phytoplankton growth responses were population specific and Phyto 13 (5.5. µm) in W2 even showed

725   reduced abundances for the F and TF treatments, underscoring the multifaceted factors controlling phytoplankton

726   dynamics and emphasizing the importance of understanding how trace metal concentrations and climate change

727   influence the marine ecosystems in the Southern Ocean.

728

729

730 **5. Conclusions**

731 Our study stands out that it combined chemistry and biology, Chl *a*, and population abundance to examine co-

732 effects using natural Antarctic phytoplankton communities at environmentally realistic Fe concentrations (+ 2

733 nM) and a predicted (2 °C) temperature increase (Boyd et al., 2015; Jabre et al., 2021; Andrew et al., 2022). So

734 far, studies investigating combined effects using natural Antarctic phytoplankton communities focussed on the

735 Ross Sea and tested 3 – 6 °C warming (Rose et al., 2009; Jabre et al., 2021). Our bioassays incubations were

736 performed under trace metal clean conditions (the entire duration) and with temperature remaining stable over the

737 course of incubations (maximum fluctuation of temperature ± 0.3 °C). We stress the importance of trace metal

738 clean working conditions to avoid inadvertently assigning Fe addition effects on phytoplankton to temperature

739 when working in low Fe regions (i.e. Southern Ocean, but also open oceans in general). The differences we found

740 between the F and TF treatment may have been assigned to temperature alone under non-trace metal clean working

741 conditions (as Fe would inadvertently have been introduced), whilst our results show that temperature alone did

742 not have a (major) effect.

743 In general, the addition of Fe was the primary factor for observed stimulatory effects. In particular, large diatoms

744 benefitted from Fe addition, although several smaller-sized phytoplankton populations showed enhanced

745 abundances upon Fe addition. Given that the intensity of the observed effects varied between the experiments

746 with distinctly different phytoplankton communities, this study emphasizes the need for studying diverse regions

747 of the Southern Ocean to better understand and predict potential future changes, especially as future changes in

748 Fe availability are region-specific (Tagliabue et al., 2016; Van Manen et al., 2022). Factors such as the dFe

749 concentrations, other trace metal concentrations which may potentially co-limit phytoplankton growth, and light

750 availability, should also be considered when studying the effects of future climate on Antarctic phytoplankton.

751 Moreover, the time of the year affects the starting composition of the phytoplankton community, and the sequence

752 of the treatments in case of dual treatments (Fe addition and temperature increase) may affect the responses

753 (Brooks and Crowe 2019), hence these factors should be considered.

754 Depending on the geographical region and the time in the productive season (Thomalla et al., 2023), global

755 warming is predicted to increase wind-induced mixing or strengthen vertical stratification (Bronselaer et al., 2020;

756 De Lavergne et al., 2014; Hillenbrand & Cortese, 2006; Shi et al., 2020). Phytoplankton will bloom earlier in the

757 productive season as a result of decreasing sea ice and consequently higher light (Krumhardt et al., 2022), rapidly

758 drawing down available Fe, followed by stratification, and thus favourable conditions for smaller-sized

759 phytoplankton (Deppeler & Davidson, 2017; Krumhardt et al., 2022). Our study shows, however, that enhanced

760 Fe input in such regions may partly overturn this warming-induced shift, assuming macronutrients will not become

761 limiting.

762 Alterations in phytoplankton community composition and cell size, as observed in our experiments, will directly

763 affect top-down control by grazers and viral infection and consequently trophic transfer efficiency. Moreover, not

764 only the flow of organic carbon through the food web will be affected, but also the flux of organic carbon to

765 deeper layers of the ocean (biological carbon pump) depends on the phytoplankton community composition, cell

766 size and type of loss factor. We recommend that future bioassay studies consider phytoplankton gross growth,

767 grazing, and viral lysis as well. After all, the typically reported net changes in the bioassay phytoplankton

768 community are the resultant of production and losses. Both Fe as well as temperature can impact the extent of the

769 loss factors. For example, grazing rates are known to increase with temperature (Chen et al., 2012; Caron &

770 Hutchins, 2013), viral lysis may occur faster at higher temperature (Maat et al., 2017), and Fe availability can

771 affect algal virus production and infectivity (Slagter et al., 2016). Finally, potential region-specific differences in

772 the share of grazing and lysis (Mojica et al., 2016; Mojica et al., 2021; Eich et al., 2022) may influence net changes

773 in phytoplankton biomass or abundances in bioassays. The Southern Ocean biogeochemical cycling and

774 ecosystems dynamics are complex and need to be better studied in field and modelling studies. The current study

775 underlines the need for assessing consequences of near future temperature changes at environmentally relevant

776 dFe concentrations.

777

778 *Data availability:* All data presented in this paper (nutrients, trace metals, phytoplankton abundances,

779 photosynthetic efficiencies, Chl *a* concentrations, pigment based community composition, particulate organic

780 carbon and particulate organic phosphate) are included in this published article and are available under

781 https://doi.org/10.25850/nioz/7b.b.hh.

782

783 *Supplement:* The supplementary material related to this article is available online at XXX.

784

785 *Author contributions:* RM and CPDB conceptualized the study. CE, MvM, EB, SBEHP, HT, IA, JSPM and RM

786 conducted the fieldwork under the lead of RM, JJ analysed the nutrient samples for Amundsen Sea bioassays,

787 WvdP analysed the pigment samples and conducted the Chemtax analysis, CE, MvM, wrote the original draft,

788 CPDB and RM edited the paper. EB, LJ and JSPM contributed to the discussion. All authors contributed to

789 commenting on the paper.

790

791   *Competing interests:* The authors declare that they have no conflict of interest.

792

793   *Acknowledgements:* We would like to thank the captain and crew of both the R/V Araon and the R/V Polarstern,

794   as well as the expedition leaders SangHoon Lee and Olaf Boebel and all other expedition participants. Our

795   participation in R/V Polarstern expedition PS117 was funded by AWI under grant number AWI_PS117_02.

796   Furthermore, we would like to thank John Seccombe from Aquahort for his support in conceiving and building

797   the heatpumps as well as his remote support during the expeditions and Sharyn Ossebaar for nutrient

798   measurements aboard R/V Polarstern. Sven Ober and all the colleagues from NIOZ national marine facilities

799   (NMF) for the preparation of the Titan sampling system during the expeditions, as well as building the incubators

800   and their help in the expedition preparation. We are also grateful to Bob Kosters (NIOZ) for his assistance with

801   the incubators, ensuring they maintained the correct temperature throughout our study. Patrick Laan (NIOZ) for

802   helping with the ICP-MS analyses, Flora Wille (NIOZ) for helping with the particulate metal analysis and Piet ter

803   Schure and his team (DMT Marine Equipment) for supplying a winch system last minute for the Titan sampling

804   system used on the R/V Araon.

805

806   *Financial support:* This work was part of the FePhyrus project (ALWPP.2016.020), which was supported by the

807   Netherlands Polar Programme (NPP), with financial aid from the Dutch Research Council (NWO). Mathijs van

808   Manen was supported by the Utrecht University-NIOZ collaboration. The ANA-08B expedition was supported

809   by the Korea Polar Research Institute grant KOPRI PE24110. The PS117 expedition was supported by the

810   auxiliary use proposal AWI_PS117_02. EMB was supported by an NSERC Canada Research Chair.

811 **References**

812 Aflenzer, H., Hoffmann, L., Holmes, T., Wuttig, K., Genovese, C., & Bowie, A. R. (2023). Effect of dissolved

813   iron (II) and temperature on growth of the Southern Ocean phytoplankton species *Fragilariopsis*

814   *cylindrus* and *Phaeocystis antarctica . Polar Biology*, *46*(11), 1163–1173.

815   https://doi.org/10.1007/s00300-023-03191-z

816 Alderkamp, A.-C., van Dijken, G. L., Lowry, K. E., Connelly, T. L., Lagerström, M., Sherrell, R. M., Haskins,

817   C., Rogalsky, E., Schofield, O., Stammerjohn, S. E., Yager, P. L., & Arrigo, K. R. (2015). Fe

818   availability drives phytoplankton photosynthesis rates during spring bloom in the Amundsen Sea

819   Polynya, Antarctica. *Elementa: Science of the Anthropocene*, *3*(C), 000043.

820   https://doi.org/10.12952/journal.elementa.000043

821 Alderkamp, A.-C., Van Dijken, G. L., Lowry, K. E., Lewis, K. M., Joy-Warren, H. L., Van De Poll, W., Laan,

822   P., Gerringa, L., Delmont, T. O., Jenkins, B. D., & Arrigo, K. R. (2019). Effects of iron and light

823   availability on phytoplankton photosynthetic properties in the Ross Sea. *Marine Ecology Progress*

824   *Series*, *621*, 33–50. Scopus. https://doi.org/10.3354/meps13000

825 Alfred-Wegener-Institut Helmholtz-Zentrum für Polar- und Meeresforschung. (2017). Polar Research and

826   Supply Vessel POLARSTERN Operated by the Alfred-Wegener-Institute. *Journal of large-scale*

827   *research facilities, 3*, A119. http://dx.doi.org/10.17815/jlsrf-3-163

828 Andrew, S. M., Morell, H. T., Strzepek, R. F., Boyd, P. W., & Ellwood, M. J. (2019). Iron availability

829   influences the tolerance of southern ocean phytoplankton to warming and elevated irradiance. *Frontiers*

830   *in Marine Science*, *6*, 681.

831 Andrew, S. M., Strzepek, R. F., M. Whitney, S., Chow, W. S., & Ellwood, M. J. (2022). Divergent

832   physiological and molecular responses of light- and iron-limited Southern Ocean phytoplankton.

833   *Limnology and Oceanography Letters*, *7*(2), 150–158. https://doi.org/10.1002/lol2.10223

834 Annett, A. L., Skiba, M., Henley, S. F., Venables, H. J., Meredith, M. P., Statham, P. J., & Ganeshram, R. S.

835   (2015). Comparative roles of upwelling and glacial iron sources in Ryder Bay, coastal western

836   Antarctic Peninsula. *Marine Chemistry*, *176*, 21–33.

837 Arrigo, K. R., & van Dijken, G. L. (2003). Phytoplankton dynamics within 37 Antarctic coastal polynya

838   systems. *Journal of Geophysical Research: Oceans*, *108*(8), 27-1-27–18.

839   https://doi.org/10.1029/2002jc001739

840 Arrigo, K. R., van Dijken, G. L., Alderkamp, A.-C., Erickson, Z. K., Lewis, K. M., Lowry, K. E., Joy-Warren,

841   H. L., Middag, R., Nash-Arrigo, J. E., Selz, V., & van de Poll, W. (2017). Early Spring Phytoplankton

842   Dynamics in the Western Antarctic Peninsula. *Journal of Geophysical Research: Oceans*, *122*(12),

843   9350–9369. https://doi.org/10.1002/2017JC013281

844 Assmy, P., Smetacek, V., Montresor, M., Klaas, C., Henjes, J., Strass, V. H., Arrieta, J. M., Bathmann, U., Berg,

845   G. M., & Breitbarth, E. (2013). Thick-shelled, grazer-protected diatoms decouple ocean carbon and

846   silicon cycles in the iron-limited Antarctic Circumpolar Current. *Proceedings of the National Academy*

847   *of Sciences*, *110*(51), 20633–20638.

848 Balaguer, J., Koch, F., Hassler, C., & Trimborn, S. (2022). Iron and manganese co-limit the growth of two

849   phytoplankton groups dominant at two locations of the Drake Passage. *Communications Biology*, *5*(1),

850   Article 1. https://doi.org/10.1038/s42003-022-03148-8

851 Basterretxea, G., Font-Muñoz, J. S., Hernández-Carrasco, I., & Sañudo-Wilhelmy, S. A. (2023). Global

852   variability of high-nutrient low-chlorophyll regions using neural networks and wavelet coherence

853   analysis. *Ocean Science*, *19*(4), 973–990. https://doi.org/10.5194/os-19-973-2023

854 Bazzani, E., Lauritano, C., & Saggiomo, M. (2023). Southern Ocean Iron Limitation of Primary Production

855   between Past Knowledge and Future Projections. *Journal of Marine Science and Engineering*, *11*(2),

856   272.

857 Bertrand, E. M., Saito, M. A., Lee, P. A., Dunbar, R. B., Sedwick, P. N., & Ditullio, G. R. (2011). Iron

858   limitation of a springtime bacterial and phytoplankton community in the Ross Sea: Implications for

859   vitamin B12 nutrition. *Frontiers in Microbiology*, *2*(AUG). Scopus.

860   https://doi.org/10.3389/fmicb.2011.00160

861 Bertrand, E. M., Saito, M. A., Rose, J. M., Riesselman, C. R., Lohan, M. C., Noble, A. E., Lee, P. A., &

862   DiTullio, G. R. (2007). Vitamin B12 and iron colimitation of phytoplankton growth in the Ross Sea.

863   *Limnology and Oceanography*, *52*(3), 1079–1093.

864 Biggs, T. E., Alvarez-Fernandez, S., Evans, C., Mojica, K. D., Rozema, P. D., Venables, H. J., Pond, D. W., &

865   Brussaard, C. P. (2019). Antarctic phytoplankton community composition and size structure:

866   Importance of ice type and temperature as regulatory factors. *Polar Biology*, *42*, 1997–2015.

867 Boyd, P. W. (2002). The role of iron in the biogeochemistry of the Southern Ocean and equatorial Pacific: A

868   comparison of in situ iron enrichments. *Deep Sea Research Part II: Topical Studies in Oceanography*,

869   *49*(9–10), 1803–1821.

870   Boyd, P. W., Arrigo, K. R., Strzepek, R., & Van Dijken, G. L. (2012). Mapping phytoplankton iron utilization:

871   Insights into Southern Ocean supply mechanisms. *Journal of Geophysical Research: Oceans*, *117*(C6).

872   Boyd, P. W., Rynearson, T. A., Armstrong, E. A., Fu, F., Hayashi, K., Hu, Z., Hutchins, D. A., Kudela, R. M.,

873   Litchman, E., & Mulholland, M. R. (2013). Marine phytoplankton temperature versus growth

874   responses from polar to tropical waters–outcome of a scientific community-wide study. *PloS One*, *8*(5),

875   e63091.

876   Boyd, P. W., Strzepek, R. F., Ellwood, M. J., Hutchins, D. A., Nodder, S. D., Twining, B. S., & Wilhelm, S. W.

877   (2015). Why are biotic iron pools uniform across high- and low-iron pelagic ecosystems? *Global*

878   *Biogeochemical Cycles*, *29*(7), 1028–1043. https://doi.org/10.1002/2014GB005014

879   Brooks, P. R., & Crowe, T. P. (2019). Combined effects of multiple stressors: New insights into the influence of

880   timing and sequence. *Frontiers in Ecology and Evolution, 7*, 387.

881   Bronselaer, B., Russell, J. L., Winton, M., Williams, N. L., Key, R. M., Dunne, J. P., Feely, R. A., Johnson, K.

882   S., & Sarmiento, J. L. (2020). Importance of wind and meltwater for observed chemical and physical

883   changes in the Southern Ocean. *Nature Geoscience*, *13*(1), 35–42. https://doi.org/10.1038/s41561-019-

884   0502-8

885   Browning, T. J., Achterberg, E. P., Engel, A., & Mawji, E. (2021). Manganese co-limitation of phytoplankton

886   growth and major nutrient drawdown in the Southern Ocean. *Nature Communications*, *12*(1), Article 1.

887   https://doi.org/10.1038/s41467-021-21122-6

888   Buesseler, K. O., Boyd, P. W., Black, E. E., & Siegel, D. A. (2020). Metrics that matter for assessing the ocean

889   biological carbon pump. *Proceedings of the National Academy of Sciences*, *117*(18), 9679–9687.

890   https://doi.org/10.1073/pnas.1918114117

891   Burns, S. M., Bundy, R. M., Abbott, W., Abdala, Z., Sterling, A. R., Chappell, P. D., Jenkins, B. D., & Buck, K.

892   N. (2023). Interactions of bioactive trace metals in shipboard Southern Ocean incubation experiments.

893   *Limnology and Oceanography*, *68*(3), 525–543. https://doi.org/10.1002/lno.12290

894   Caron, D. A., & Hutchins, D. A. (2013). The effects of changing climate on microzooplankton grazing and

895   community structure: Drivers, predictions and knowledge gaps. *Journal of Plankton Research*, *35*(2),

896   235–252. https://doi.org/10.1093/plankt/fbs091

897   Chen, B., Landry, M. R., Huang, B., & Liu, H. (2012). Does warming enhance the effect of microzooplankton

898   grazing on marine phytoplankton in the ocean? *Limnology and Oceanography*, *57*(2), 519–526.

899   Cullen, J. T., & Sherrell, R. M. (1999). Techniques for determination of trace metals in small samples of size-

900   fractionated particulate matter: Phytoplankton metals off central California. *Marine Chemistry*, *67*(3–

901   4), 233–247.

902   Cunningham, B. R., & John, S. G. (2017). The effect of iron limitation on cyanobacteria major nutrient and

903   trace element stoichiometry. *Limnology and Oceanography*, *62*(2), 846–858.

904   https://doi.org/10.1002/lno.10484

905   Cutter, G. A., Andersson, P., Codispoti, L., Croot, P., Place, P., Hoe, T., Kingdom, U., Francois, R., Sciences,

906   O., Lohan, M., Circus, D., & Obata, H. (2017). *Sampling and Sample-handling Protocols for*

907   *GEOTRACES Cruises*. *3.0*(August).

908   Darelius, E., Daae, K., Dundas, V., Fer, I., Hellmer, H. H., Janout, M., Nicholls, K. W., Sallée, J.-B., &

909   Østerhus, S. (2023). Observational evidence for on-shelf heat transport driven by dense water export in

910   the Weddell Sea. *Nature Communications*, *14*(1), 1022.

911   De Baar, H. J. W., Boyd, P. W., Coale, K. H., Landry, M. R., Tsuda, A., Assmy, P., Bakker, D. C. E., Bozec, Y.,

912   Barber, R. T., Brzezinski, M. A., Buesseler, K. O., Boyé, M., Croot, P. L., Gervais, F., Gorbunov, M.

913   Y., Harrison, P. J., Hiscock, W. T., Laan, P., Lancelot, C., … Wong, C. (2005). Synthesis of iron

914   fertilization experiments: From the Iron Age in the Age of Enlightenment. *Journal of Geophysical*

915   *Research: Oceans*, *110*(C9), 2004JC002601. https://doi.org/10.1029/2004JC002601

916   De Baar, H. J. W., Timmermans, K. R., Laan, P., De Porto, H. H., Ober, S., Blom, J. J., Bakker, M. C.,

917   Schilling, J., Sarthou, G., Smit, M. G., & Klunder, M. (2008). Titan: A new facility for ultraclean

918   sampling of trace elements and isotopes in the deep oceans in the international Geotraces program.

919   *Marine Chemistry*, *111*(1–2), 4–21. https://doi.org/10.1016/j.marchem.2007.07.009

920   De Lavergne, C., Palter, J. B., Galbraith, E. D., Bernardello, R., & Marinov, I. (2014). Cessation of deep

921   convection in the open Southern Ocean under anthropogenic climate change. *Nature Climate Change*,

922   *4*(4), 278–282.

923   Deppeler, S. L., & Davidson, A. T. (2017). Southern Ocean Phytoplankton in a Changing Climate. *Frontiers in*

924   *Marine Science*, *4*. https://www.frontiersin.org/articles/10.3389/fmars.2017.00040

925   Drijfhout, S. S., Bull, C. Y. S., Hewitt, H., Holland, P. R., Jenkins, A., Mathiot, P., & Garabato, A. N. (2024).

926   An Amundsen Sea source of decadal temperature changes on the Antarctic continental shelf. *Ocean*

927   *Dynamics*, *74*(1), 37–52. https://doi.org/10.1007/s10236-023-01587-3

928   Eich, C., Biggs, T. E., van de Poll, W. H., van Manen, M., Tian, H.-A., Jung, J., Lee, Y., Middag, R., &

929   Brussaard, C. P. (2022). Ecological importance of viral lysis as a loss factor of phytoplankton in the

930   Amundsen Sea. *Microorganisms*, *10*(10), 1967.

931   Eich, C., Pont, S. B., & Brussaard, C. P. (2021). Effects of UV radiation on the chlorophyte *Micromonas polaris*

932   host–virus interactions and MpoV-45T virus infectivity. *Microorganisms*, *9*(12), 2429.

933   Fahrbach, E., Hoppema, M., Rohardt, G., Schröder, M., & Wisotzki, A. (2004). Decadal-scale variations of

934   water mass properties in the deep Weddell Sea. *Ocean Dynamics*, *54*(1), 77–91.

935   https://doi.org/10.1007/s10236-003-0082-3

936   Feng, Y., Hare, C. E., Rose, J. M., Handy, S. M., DiTullio, G. R., Lee, P. A., Smith, W. O., Peloquin, J., Tozzi,

937   S., Sun, J., Zhang, Y., Dunbar, R. B., Long, M. C., Sohst, B., Lohan, M., & Hutchins, D. A. (2010).

938   Interactive effects of iron, irradiance and CO2 on Ross Sea phytoplankton. *Deep-Sea Research Part I:*

939   *Oceanographic Research Papers*, *57*(3), 368–383. https://doi.org/10.1016/j.dsr.2009.10.013

940   Fisher, B. J., Poulton, A. J., Meredith, M. P., Baldry, K., Schofield, O., & Henley, S. F. (2023).

941   Biogeochemistry of climate driven shifts in Southern Ocean primary producers. *Biogeosciences*

942   *Discussions*, 1–29.

943   Fourquez, M., Janssen, D. J., Conway, T. M., Cabanes, D., Ellwood, M. J., Sieber, M., Trimborn, S., & Hassler,

944   C. (2023). Chasing iron bioavailability in the Southern Ocean: Insights from *Phaeocystis antarctica*

945   and iron speciation. *Science Advances*, *9*(26), eadf9696. https://doi.org/10.1126/sciadv.adf9696

946   Friedlingstein, P., O'sullivan, M., Jones, M. W., Andrew, R. M., Gregor, L., Hauck, J., Le Quéré, C., Luijkx, I.

947   T., Olsen, A., & Peters, G. P. (2022). Global carbon budget 2022. *Earth System Science Data*

948   *Discussions*, *2022*, 1–159.

949   From, N., Richardson, K., Mousing, E. A., & Jensen, P. E. (2014). Removing the light history signal from

950   normalized variable fluorescence (F $_v$ /F $_m$) measurements on marine phytoplankton. *Limnology and*

951   *Oceanography: Methods*, *12*(11), 776–783. https://doi.org/10.4319/lom.2014.12.776

952   Garrison, D. L., Gowing, M. M., Hughes, M. P., Campbell, L., Caron, D. A., Dennett, M. R., Shalapyonok, A.,

953   Olson, R. J., Landry, M. R., Brown, S. L., Liu, H.-B., Azam, F., Steward, G. F., Ducklow, H. W., &

954   Smith, D. C. (2000). Microbial food web structure in the Arabian Sea: A US JGOFS study. *Deep Sea*

955   *Research Part II: Topical Studies in Oceanography*, *47*(7), 1387–1422. https://doi.org/10.1016/S0967-

956   0645(99)00148-4

957   Geider, R. J. (1987). Light and temperature dependence of the carbon to chlorophyll a ratio in microalgae and

958   cyanobacteria: Implications for physiology and growth of phytoplankton. *New Phytologist*, 1–34.

959   Geider, R. J., & La Roche, J. (1994). The role of iron in phytoplankton photosynthesis, and the potential for

960   iron-limitation of primary productivity in the sea. *Photosynthesis Research*, *39*, 275–301.

961   Geider, R. J., MacIntyre, H. L., & Kana, T. M. (1998). A dynamic regulatory model of phytoplanktonic

962   acclimation to light, nutrients, and temperature. *Limnology and Oceanography*, *43*(4), 679–694.

963   Gerringa, L. J. A., Alderkamp, A.-C., Laan, P., Thuróczy, C.-E., De Baar, H. J. W., Mills, M. M., van Dijken,

964   G. L., van Haren, H., & Arrigo, K. R. (2020). Corrigendum to" Iron from melting glaciers fuels the

965   phytoplankton blooms in Amundsen Sea (Southern Ocean): Iron biogeochemistry"(Gerringa et al.,

966   2012). *Deep Sea Research Part II: Topical Studies in Oceanography*, *177*, 104843.

967   Gerringa, L. J. A., Laan, P., Arrigo, K. R., van Dijken, G. L., & Alderkamp, A.-C. (2019). The organic

968   complexation of iron in the Ross sea. *Marine Chemistry*, *215*, 103672.

969   https://doi.org/10.1016/j.marchem.2019.103672

970   Gerringa, L. J., Alderkamp, A.-C., Laan, P., Thuroczy, C.-E., De Baar, H. J., Mills, M. M., van Dijken, G. L.,

971   van Haren, H., & Arrigo, K. R. (2012). Iron from melting glaciers fuels the phytoplankton blooms in

972   Amundsen Sea (Southern Ocean): Iron biogeochemistry. *Deep Sea Research Part II: Topical Studies in*

973   *Oceanography*, *71*, 16–31.

974   Gómez-Valdivia, F., Holland, P. R., Siahaan, A., Dutrieux, P., & Young, E. (2023). Projected West Antarctic

975   Ocean Warming Caused by an Expansion of the Ross Gyre. *Geophysical Research Letters*, *50*(6),

976   e2023GL102978. https://doi.org/10.1029/2023GL102978

977   Gordon, L. I., Jennings Jr, J. C., Ross, A. A., & Krest, J. M. (1993). A suggested protocol for continuous flow

978   automated analysis of seawater nutrients (phosphate, nitrate, nitrite and silicic acid) in the WOCE

979   Hydrographic Program and the Joint Global Ocean Fluxes Study. *WOCE Hydrographic Program*

980   *Office, Methods Manual WHPO*, *68/91*, 1–52.

981   Greene, R. M., Geider, R. J., Kolber, Z., & Falkowski, P. G. (1992). Iron-induced changes in light harvesting

982   and photochemical energy conversion processes in eukaryotic marine algae. *Plant Physiology*, *100*(2),

983   565–575.

984   Hassler, C. S., & Schoemann, V. (2009). Bioavailability of organically bound Fe to model phytoplankton of the

985   Southern Ocean. *Biogeosciences*, *6*(10), 2281–2296.

986   Hawco, N. J., Tagliabue, A., & Twining, B. S. (2022). Manganese Limitation of Phytoplankton Physiology and

987   Productivity in the Southern Ocean. *Global Biogeochemical Cycles*, *36*(11), e2022GB007382.

988   https://doi.org/10.1029/2022GB007382

989   Hillenbrand, C.-D., & Cortese, G. (2006). Polar stratification: A critical view from the Southern Ocean.

990   *Palaeogeography, Palaeoclimatology, Palaeoecology*, *242*(3–4), 240–252.

991   Hinz, D. J., Nielsdóttir, M. C., Korb, R. E., Whitehouse, M. J., Poulton, A. J., Moore, C. M., Achterberg, E. P.,

992   & Bibby, T. S. (2012). Responses of microplankton community structure to iron addition in the Scotia

993   Sea. *Deep-Sea Research Part II: Topical Studies in Oceanography*, *59–60*, 36–46.

994   https://doi.org/10.1016/j.dsr2.2011.08.006

995   Hopwood, M. J., Carroll, D., Höfer, J., Achterberg, E. P., Meire, L., Le Moigne, F. A., Bach, L. T., Eich, C.,

996   Sutherland, D. A., & González, H. E. (2019). Highly variable iron content modulates iceberg-ocean

997   fertilisation and potential carbon export. *Nature Communications*, *10*(1), 5261.

998   Huang, Y., Fassbender, A. J., & Bushinsky, S. M. (2023). Biogenic carbon pool production maintains the

999   Southern Ocean carbon sink. *Proceedings of the National Academy of Sciences*, *120*(18),

1000   e2217909120. https://doi.org/10.1073/pnas.2217909120

1001   Hutchins, D. A., & Boyd, P. W. (2016). Marine phytoplankton and the changing ocean iron cycle. *Nature*

1002   *Climate Change*, *6*(12), 1072–1079.

1003   Hutchins, D. A., & Bruland, K. W. (1998). Iron-limited diatom growth and Si:N uptake ratios in a coastal

1004   upwelling regime. *Nature*, *393*(6685), 561–564. Scopus. https://doi.org/10.1038/31203

1005   Jabre, L., & Bertrand, E. M. (2020). Interactive effects of iron and temperature on the growth of *Fragilariopsis*

1006   *cylindrus* . *Limnology and Oceanography Letters*, *5*(5), 363–370.

1007   Jabre, L. J., Allen, A. E., McCain, J. S. P., McCrow, J. P., Tenenbaum, N., Spackeen, J. L., Sipler, R. E., Green,

1008   B. R., Bronk, D. A., Hutchins, D. A., & Bertrand, E. M. (2021). Molecular underpinnings and

1009   biogeochemical consequences of enhanced diatom growth in a warming Southern Ocean. *Proceedings*

1010   *of the National Academy of Sciences*, *118*(30), e2107238118. https://doi.org/10.1073/pnas.2107238118

1011   Jensen, L. T., Wyatt, N. J., Landing, W. M., & Fitzsimmons, J. N. (2020). Assessment of the stability, sorption,

1012   and exchangeability of marine dissolved and colloidal metals. *Marine Chemistry*, *220*, 103754.

1013   https://doi.org/10.1016/j.marchem.2020.103754

1014   Jeon, M. H., Jung, J., Park, M. O., Aoki, S., Kim, T.-W., & Kim, S.-K. (2021). Tracing Circumpolar Deep

1015   Water and glacial meltwater using humic-like fluorescent dissolved organic matter in the Amundsen

1016   Sea, Antarctica. *Marine Chemistry*, *235*, 104008. https://doi.org/10.1016/j.marchem.2021.104008

1017   Kroh, G. E., & Pilon, M. (2020). Regulation of iron homeostasis and use in chloroplasts. *International Journal*

1018   *of Molecular Sciences*, *21*(9), 3395.

1019   Krumhardt, K. M., Long, M. C., Sylvester, Z. T., & Petrik, C. M. (2022). Climate drivers of Southern Ocean

1020   phytoplankton community composition and potential impacts on higher trophic levels. *Frontiers in*

1021   *Marine Science*, *9*, 916140.

1022   Kustka, A. B., Allen, A. E., & Morel, F. M. (2007). Sequence analysis and transcriptional regulation of iron

1023   acquisition genes in two marine diatoms 1. *Journal of Phycology*, *43*(4), 715–729.

1024   Lampe, R. H., Mann, E. L., Cohen, N. R., Till, C. P., Thamatrakoln, K., Brzezinski, M. A., Bruland, K. W.,

1025   Twining, B. S., & Marchetti, A. (2018). Different iron storage strategies among bloom-forming

1026   diatoms. *Proceedings of the National Academy of Sciences*, *115*(52), E12275–E12284.

1027   https://doi.org/10.1073/pnas.1805243115

1028   Lane, E. S., Jang, K., Cullen, J. T., & Maldonado, M. T. (2008). The interaction between inorganic iron and

1029   cadmium uptake in the marine diatom Thalassiosira oceanica. *Limnology and Oceanography*, *53*(5),

1030   1784–1789.

1031   Lannuzel, D., Vancoppenolle, M., van Der Merwe, P., De Jong, J., Meiners, K. M., Grotti, M., Nishioka, J., &

1032   Schoemann, V. (2016). Iron in sea ice: Review and new insights. *Elementa*, *4*, 000130.

1033   Laws, E. A., & Bannister, T. T. (1980). Nutrient-and light-limited growth of Thalassiosira fluviatilis in

1034   continuous culture, with implications for phytoplankton growth in the ocean 1. *Limnology and*

1035   *Oceanography*, *25*(3), 457–473.

1036   Maat, D. S., Biggs, T., Evans, C., Van Bleijswijk, J. D. L., Van der Wel, N. N., Dutilh, B. E., & Brussaard, C. P.

1037   D. (2017). Characterization and Temperature Dependence of Arctic *Micromonas polaris*Viruses.

1038   *Viruses*, *9*(6), Article 6. https://doi.org/10.3390/v9060134

1039   Mackey, M. D., Mackey, D. J., Higgins, H. W., & Wright, S. W. (1996). CHEMTAX-a program for estimating

1040   class abundances from chemical markers: Application to HPLC measurements of phytoplankton.

1041   *Marine Ecology Progress Series*, *144*, 265–283.

1042   Marie, D., Partensky, F., Vaulot, D., & Brussaard, C. P. D. (1999). Enumeration of phytoplankton, bacteria, and

1043   viruses in marine samples. *Current Protocols in Cytometry*. https://doi.org/10.1002/0471142956

1044   Martin, J. H., Fitzwater, S. E., & Gordon, R. M. (1990). Iron deficiency limits phytoplankton growth in

1045   Antarctic waters. *Global Biogeochemical Cycles*, *4*(1), 5–12.

1046   McCain, J. S. P., Tagliabue, A., Susko, E., Achterberg, E. P., Allen, A. E., & Bertrand, E. M. (2021). Cellular

1047   costs underpin micronutrient limitation in phytoplankton. *Science Advances*, *7*(32), eabg6501.

1048   https://doi.org/10.1126/sciadv.abg6501

1049   Meredith, M., M. Sommerkorn, S. Cassotta, C. Derksen, A. Ekaykin, A. Hollowed, G. Kofinas, A. Mackintosh,

1050   J. Melbourne-Thomas, M.M.C. Muelbert, G. Ottersen, H. Pritchard, and E.A.G. Schuur. (2019).

1051   *Chapter 3: IPCC Polar regions — Special Report on the Ocean and Cryosphere in a Changing*

1052   *Climate*. https://www.ipcc.ch/srocc/chapter/chapter-3-2/

1053   Meyerink, S. W., Ellwood, M. J., Maher, W. A., Dean Price, G., & Strzepek, R. F. (2017). Effects of iron

1054   limitation on silicon uptake kinetics and elemental stoichiometry in two Southern Ocean diatoms,

1055   *Eucampia antarctica* and *Proboscia inermis* , and the temperate diatom *Thalassiosira pseudonana*.

1056   *Limnology and Oceanography*, *62*(6), 2445–2462.

1057   Middag, R., De Baar, H. J., Bruland, K. W., & Van Heuven, S. M. (2020). The distribution of nickel in the

1058   West-Atlantic Ocean, its relationship with phosphate and a comparison to cadmium and zinc. *Frontiers*

1059   *in Marine Science*, *7*, 105.

1060   Middag, R., Zitoun, R., & Conway, T. (2023). Trace Metals. In J. Blasco & A. Tovar-Sánchez (Eds.), *Marine*

1061   *Analytical Chemistry* (pp. 103–198). Springer International Publishing. https://doi.org/10.1007/978-3-

1062   031-14486-8_3

1063   Mills, M. M., Alderkamp, A. C., Thuróczy, C. E., van Dijken, G. L., Laan, P., de Baar, H. J. W., & Arrigo, K.

1064   R. (2012). Phytoplankton biomass and pigment responses to Fe amendments in the Pine Island and

1065   Amundsen polynyas. *Deep-Sea Research Part II: Topical Studies in Oceanography*, *71–76*(3), 61–76.

1066   https://doi.org/10.1016/j.dsr2.2012.03.008

1067   Minas, H. J., & Minas, M. (1992). Net community production in High nutrient-low chlorophyll waters of the

1068   tropical and Antarctic oceans-grazing vs iron hypothesis. *Oceanologica Acta*, *15*(2), 145–162.

1069   Moore, J. K., Fu, W., Primeau, F., Britten, G. L., Lindsay, K., Long, M., Doney, S. C., Mahowald, N., Hoffman,

1070   F., & Randerson, J. T. (2018). Sustained climate warming drives declining marine biological

1071   productivity. *Science*, *359*(6380), 1139–1143. https://doi.org/10.1126/science.aao6379

1072   Morán, X. A. G., Sebastián, M., Pedrís-Alií, C., & Estrada, M. (2006). Response of Southern Ocean

1073   phytoplankton and bacterioplankton production to short-term experimental warming. *Limnology and*

1074   *Oceanography*, *51*(4), 1791–1800. https://doi.org/10.4319/lo.2006.51.4.1791

1075   Morrison, A. K., England, M. H., Hogg, A. McC., & Kiss, A. E. (2023). Weddell Sea Control of Ocean

1076   Temperature Variability on the Western Antarctic Peninsula. *Geophysical Research Letters*, *50*(15),

1077   e2023GL103018. https://doi.org/10.1029/2023GL103018

1078   Noiri, Y., Kudo, I., Kiyosawa, H., Nishioka, J., & Tsuda, A. (2005). Influence of iron and temperature on

1079   growth, nutrient utilization ratios and phytoplankton species composition in the western subarctic

1080   Pacific Ocean during the SEEDS experiment. *Progress in Oceanography*, *64*(2–4), 149–166.

1081   https://doi.org/10.1016/j.pocean.2005.02.006

1082   Ohnemus, D. C., Auro, M. E., Sherrell, R. M., Lagerström, M., Morton, P. L., Twining, B. S., Rauschenberg, S.,

1083   & Lam, P. J. (2014). Laboratory intercomparison of marine particulate digestions including Piranha: A

1084   novel chemical method for dissolution of polyethersulfone filters. *Limnology and Oceanography:*

1085   *Methods*, *12*(8), 530–547.

1086   Olson, R. J., Sosik, H. M., Chekalyuk, A. M., & Shalapyonok, A. (2000). Effects of iron enrichment on

1087   phytoplankton in the Southern Ocean during late summer: Active fluorescence and flow cystometric

1088   analyses. *Deep-Sea Research Part II: Topical Studies in Oceanography*, *47*(15–16), 3181–3200.

1089   Scopus. https://doi.org/10.1016/S0967-0645(00)00064-3

1090   Pausch, F., Bischof, K., & Trimborn, S. (2019). Iron and manganese co-limit growth of the Southern Ocean

1091   diatom Chaetoceros debilis. *PLOS ONE*, *14*(9), e0221959.

1092   https://doi.org/10.1371/journal.pone.0221959

1093   Peers, G., & Price, N. M. (2004). A role for manganese in superoxide dismutases and growth of iron-deficient

1094   diatoms. *Limnology and Oceanography*, *49*(5), 1774–1783. https://doi.org/10.4319/lo.2004.49.5.1774

1095   Planquette, H., & Sherrell, R. M. (2012). Sampling for particulate trace element determination using water

1096   sampling bottles: Methodology and comparison to in situ pumps. *Limnology and Oceanography:*

1097   *Methods*, *10*(5), 367–388.

1098   Primeau, F. W., Holzer, M., & DeVries, T. (2013). Southern Ocean nutrient trapping and the efficiency of the

1099   biological pump. *Journal of Geophysical Research: Oceans*, *118*(5), 2547–2564.

1100   https://doi.org/10.1002/jgrc.20181

1101 R Core Team. (2021). *R: A language and environment for statistical computing.* (4.1.0). R Foundation for

1102 Statistical Computing.

1103 Reay, D. S., Priddle, J., Nedwell, D. B., Whitehouse, M. J., Ellis-Evans, J. C., Deubert, C., & Connelly, D. P.

1104 (2001). Regulation by low temperature of phytoplankton growth and nutrient uptake in the Southern

1105 Ocean. *Marine Ecology Progress Series*, *219*, 51–64.

1106 Rignot, E., Jacobs, S., Mouginot, J., & Scheuchl, B. (2013). Ice-Shelf Melting Around Antarctica. *Science*,

1107 *341*(6143), 266–270. https://doi.org/10.1126/science.1235798

1108 Rijkenberg, M. J. A., de Baar, H. J. W., Bakker, K., Gerringa, L. J. A., Keijzer, E., Laan, M., Laan, P., Middag,

1109 R., Ober, S., van Ooijen, J., Ossebaar, S., van Weerlee, E. M., & Smit, M. G. (2015). 'PRISTINE', a

1110 new high volume sampler for ultraclean sampling of trace metals and isotopes. *Marine Chemistry*,

1111 *177*(October 2017), 501–509. https://doi.org/10.1016/j.marchem.2015.07.001

1112 Rose, J. M., Feng, Y., DiTullio, G. R., Dunbar, R. B., Hare, C. E., Lee, P. A., Lohan, M., Long, M., Smith Jr,

1113 W. O., & Sohst, B. (2009). Synergistic effects of iron and temperature on Antarctic phytoplankton and

1114 microzooplankton assemblages. *Biogeosciences*, *6*(12), 3131–3147.

1115 Ryan-Keogh, T. J., Thomalla, S. J., Monteiro, P. M., & Tagliabue, A. (2023). Multidecadal trend of increasing

1116 iron stress in Southern Ocean phytoplankton. *Science*, *379*(6634), 834–840.

1117 Ryderheim, F., Grønning, J., & Kiørboe, T. (2022). Thicker shells reduce copepod grazing on diatoms.

1118 *Limnology and Oceanography Letters*, *7*(5), 435–442.

1119 Sarmiento, J. L., Gruber, N., Brzezinski, M. A., & Dunne, J. P. (2004). High-latitude controls of thermocline

1120 nutrients and low latitude biological productivity. *Nature*, *427*(6969), Article 6969.

1121 https://doi.org/10.1038/nature02127

1122 Scharek, R., Van Leeuwe, M. A., & De Baar, H. J. W. (1997). Responses of Southern Ocean phytoplankton to

1123 the addition of trace metals. *Deep-Sea Research Part II: Topical Studies in Oceanography*, *44*(1–2),

1124 209–227. https://doi.org/10.1016/S0967-0645(96)00074-4

1125 Schoffman, H., Lis, H., Shaked, Y., & Keren, N. (2016). Iron–Nutrient Interactions within Phytoplankton.

1126 *Frontiers in Plant Science*, *7*. https://www.frontiersin.org/articles/10.3389/fpls.2016.01223

1127 Selz, V., Lowry, K. E., Lewis, K. M., Joy-Warren, H. L., van de Poll, W., Nirmel, S., Tong, A., & Arrigo, K. R.

1128 (2018). Distribution of Phaeocystis antarctica-dominated sea ice algal communities and their potential

1129 to seed phytoplankton across the western Antarctic Peninsula in spring. *Marine Ecology Progress*

1130 *Series*, *586*, 91–112.

1131 Seyitmuhammedov, K., Stirling, C. H., Reid, M. R., van Hale, R., Laan, P., Arrigo, K. R., van Dijken, G.,

1132 Alderkamp, A.-C., & Middag, R. (2022). The distribution of Fe across the shelf of the Western

1133 Antarctic Peninsula at the start of the phytoplankton growing season. *Marine Chemistry*, *238*, 104066.

1134 Sherrell, R. M., Lagerström, M. E., Forsch, K. O., Stammerjohn, S. E., & Yager, P. L. (2015). Dynamics of

1135 dissolved iron and other bioactive trace metals (Mn, Ni, Cu, Zn) in the Amundsen Sea Polynya,

1136 Antarctica. *Elementa: Science of the Anthropocene*, *3*, 000071.

1137 https://doi.org/10.12952/journal.elementa.000071

1138 Shi, J.-R., Talley, L. D., Xie, S.-P., Liu, W., & Gille, S. T. (2020). Effects of buoyancy and wind forcing on

1139 Southern Ocean climate change. *Journal of Climate*, *33*(23), 10003–10020.

1140 Slagter, H. A., Gerringa, L. J. A., & Brussaard, C. P. D. (2016). Phytoplankton Virus Production Negatively

1141 Affected by Iron Limitation. *Frontiers in Marine Science*, *3*.

1142 https://www.frontiersin.org/articles/10.3389/fmars.2016.00156

1143 Stapleford, L. S., & Smith, R. E. (1996). The interactive effects of temperature and silicon limitation on the

1144 psychrophilic ice diatom Pseudonitszchia seriata. *Polar Biology*, *16*, 589–594.

1145 Tagliabue, A., Aumont, O., DeAth, R., Dunne, J. P., Dutkiewicz, S., Galbraith, E., Misumi, K., Moore, J. K.,

1146 Ridgwell, A., Sherman, E., Stock, C., Vichi, M., Völker, C., & Yool, A. (2016). How well do global

1147 ocean biogeochemistry models simulate dissolved iron distributions? *Global Biogeochemical Cycles*,

1148 *30*(2), 149–174. https://doi.org/10.1002/2015GB005289

1149 Tagliabue, A., Sallée, J.-B., Bowie, A. R., Lévy, M., Swart, S., & Boyd, P. W. (2014). Surface-water iron

1150 supplies in the Southern Ocean sustained by deep winter mixing. *Nature Geoscience*, *7*(4), 314–320.

1151 Takahashi, T., Sweeney, C., Hales, B., Chipman, D. W., Newberger, T., Goddard, J. G., Iannuzzi, R. A., &

1152 Sutherland, S. C. (2012). The changing carbon cycle in the Southern Ocean. *Oceanography*, *25*(3), 26–

1153 37.

1154 Teske, V., Timmermann, R., & Semmler, T. (2024). Subsurface warming in the Antarctica's Weddell Sea can

1155 be avoided by reaching the 2∘ C warming target. *Communications Earth & Environment*, *5*(1), 93.

1156 Thomalla, S. J., Nicholson, S.-A., Ryan-Keogh, T. J., & Smith, M. E. (2023). Widespread changes in Southern

1157 Ocean phytoplankton blooms linked to climate drivers. *Nature Climate Change*, *13*(9), 975–984.

1158 Twining, B. S., Baines, S. B., & Fisher, N. S. (2004). Element stoichiometries of individual plankton cells

1159 collected during the Southern Ocean Iron Experiment (SOFeX). *Limnology and Oceanography*, *49*(6),

1160 2115–2128. https://doi.org/10.4319/lo.2004.49.6.2115

1161   Van der Merwe, P., Wuttig, K., Holmes, T., Trull, T. W., Chase, Z., Townsend, A. T., Goemann, K., & Bowie,

1162   A. R. (2019). High lability Fe particles sourced from glacial erosion can meet previously unaccounted

1163   biological demand: Heard Island, Southern Ocean. *Frontiers in Marine Science*, *6*, 332.

1164   Van Heukelem, L., & Thomas, C. S. (2001). Computer-assisted high-performance liquid chromatography

1165   method development with applications to the isolation and analysis of phytoplankton pigments. *Journal*

1166   *of Chromatography A*, *910*(1), 31–49. https://doi.org/10.1016/S0378-4347(00)00603-4

1167   Van Manen, M., Aoki, S., Brussaard, C. P., Conway, T. M., Eich, C., Gerringa, L. J., Jung, J., Kim, T.-W., Lee,

1168   S., & Lee, Y. (2022). The role of the Dotson Ice Shelf and Circumpolar Deep Water as driver and

1169   source of dissolved and particulate iron and manganese in the Amundsen Sea polynya, Southern

1170   Ocean. *Marine Chemistry*, *246*, 104161.

1171   Veldhuis, M. J., & Kraay, G. W. (2004). Phytoplankton in the subtropical Atlantic Ocean: Towards a better

1172   assessment of biomass and composition. *Deep Sea Research Part I: Oceanographic Research Papers*,

1173   *51*(4), 507–530.

1174   Venables, H., & Moore, C. M. (2010). Phytoplankton and light limitation in the Southern Ocean: Learning from

1175   high-nutrient, high-chlorophyll areas. *Journal of Geophysical Research: Oceans*, *115*(C2).

1176   Verardo, D. J., Froelich, P. N., & McIntyre, A. (1990). Determination of organic carbon and nitrogen in marine

1177   sediments using the Carlo Erba NA-1500 Analyzer. *Deep Sea Research Part A. Oceanographic*

1178   *Research Papers*, *37*(1), 157–165.

1179   Viljoen, J. J., Philibert, R., Van Horsten, N., Mtshali, T., Roychoudhury, A. N., Thomalla, S., & Fietz, S.

1180   (2018). Phytoplankton response in growth, photophysiology and community structure to iron and light

1181   in the Polar Frontal Zone and Antarctic waters. *Deep-Sea Research Part I: Oceanographic Research*

1182   *Papers*, *141*, 118–129. Scopus. https://doi.org/10.1016/j.dsr.2018.09.006

1183   Waite, A. M., & Nodder, S. D. (2001). The effect of in situ iron addition on the sinking rates and export flux of

1184   Southern Ocean diatoms. *Deep Sea Research Part II: Topical Studies in Oceanography*, *48*(11–12),

1185   2635–2654.

1186   Wang, X. J., Behrenfeld, M., Le Borgne, R., Murtugudde, R., & Boss, E. (2009). Regulation of phytoplankton

1187   carbon to chlorophyll ratio by light, nutrients and temperature in the Equatorial Pacific Ocean: A basin-

1188   scale model. *Biogeosciences*, *6*(3), 391–404.

1189 Worden, A. Z., Nolan, J. K., & Palenik, B. (2004). Assessing the dynamics and ecology of marine

1190   picophytoplankton: The importance of the eukaryotic component. *Limnology and Oceanography*,

1191   *49*(1), 168–179. https://doi.org/10.4319/lo.2004.49.1.0168

1192 Wu, M., McCain, J. S. P., Rowland, E., Middag, R., Sandgren, M., Allen, A. E., & Bertrand, E. M. (2019a).

1193   Manganese and iron deficiency in Southern Ocean *Phaeocystis antarctica* populations revealed through

1194   taxon-specific protein indicators. *Nature Communications*, *10*(1), 3582.

1195   https://doi.org/10.1038/s41467-019-11426-z

1196 Yoon, J.-E., Yoo, K.-C., Macdonald, A. M., Yoon, H.-I., Park, K.-T., Yang, E. J., Kim, H.-C., Lee, J. I., Lee, M.

1197   K., Jung, J., Park, J., Lee, J., Kim, S., Kim, S.-S., Kim, K., & Kim, I.-N. (2018). Reviews and

1198   syntheses: Ocean iron fertilization experiments – past, present, and future looking to a future Korean

1199   Iron Fertilization Experiment in the Southern Ocean (KIFES) project. *Biogeosciences*, *15*(19), 5847–

1200   5889. https://doi.org/10.5194/bg-15-5847-2018

1201 Zhu, Z., Xu, K., Fu, F., Spackeen, J. L., Bronk, D. A., & Hutchins, D. A. (2016). A comparative study of iron

1202   and temperature interactive effects on diatoms and *Phaeocystis antarctica* from the Ross Sea,

1203   Antarctica. *Marine Ecology Progress Series*, *550*, 39–51.

1204